國 立 交 通 大 學

電信工程研究所

碩 士 論 文

前瞻長程演進異質性網路的頻譜與能源效率之分析

Investigation of Spectral and Energy Efficiency in LTE-A Heterogeneous Networks

研究生：謝宗展

指導教授：王蒞君

中 華 民 國 一百零一 年 六 月

前瞻長程演進異質性網路的頻譜與能源效率之分析

Investigation of Spectral and Energy Efficiency in LTE-A Heterogeneous Networks

研 究 生：謝宗展　　Student：Tsung-Chan Hsieh

指導教授：王蒞君　　Advisor：Li-Chun Wang

國 立 交 通 大 學

電信工程研究所

碩 士 論 文

A Thesis

Submitted to Institute of Communications Engineering

College of Electrical and Computer Engineering

National Chiao Tung University

in partial Fulfillment of the Requirements

for the Degree of

Master of Science

In

Communication Engineering

June 2012

Hsinchu, Taiwan, Republic of China

中華民國 一百零一 年 六 月

前瞻長程演進異質性網路的頻譜與能源效率之分析

學生：謝宗展　　指導教授：王蒞君　教授

國立交通大學

電機學院電信工程研究所

摘要

在此篇論文中，我們探討應用階層式基地台合作技術之第三代合作夥伴前瞻長程演進異質性網路系統的頻譜與能源效率。我們發現同時考慮系統架構與合作傳輸方法的設計能夠達到綠能傳輸之目的。因為基地台合作之技術可以有效降低共同通道干擾與改善接收訊號品質，且系統架構對於系統之表現有相當的影響。特別是考慮了同時結合細胞間與細胞內基地台合作之方法。這篇論文呈現了利用上述之聯合設計方法於應用階層式基地台合作技術之異質性網路系統表現的改善。模擬結果顯示，採用我們提出的聯合設計方法之異質性網路系統比起傳統單用戶多輸入多輸出系統是一個有效提高頻譜與能源效率的方法。

Investigation of Spectral and Energy Efficiency in LTE-A Heterogeneous Networks

A THESIS Presented to

The Academic Faculty By

Tsung-Chan Hsieh

In Partial Fulfillment

of the Requirements for the Degree of

Master in Communication Engineering

Institute of Communications Engineering

College of Electrical and Computer Engineering

National Chiao-Tung University

June, 2012

Copyright ©2012 by Tsung-Chan Hsieh

Abstract

In this thesis, we investigate both spectral and energy efficiency of hierarchical base station cooperation techniques in heterogeneous networks (HetNet) of the 3rd Generation Partnership Project (3GPP) Long Term Evolution-Advanced (LTE-A) system. We find that joint consideration of system architectures and cooperation schemes will achieve energy-efficient transmission. Because the co-channel interference can be mitigated significantly and the signal quality is able to be improved through base station coordination techniques, and system architectures have great impacts on the system performance. Especially, coordinated multi-point (CoMP) techniques of different levels, e.g., intra and inter-site CoMP, are considered jointly. We address the performance improvements of HetNet system with hierarchical base station coordination techniques by the joint design of both system architecture and coordinated transmission scheme. The proposed joint design methodology is a promising solution for improving spectral and energy efficiency compared to the conventional single user multi-input-multi-output (SU-MIMO) system.

Acknowledgments

Foremost, I would like to appreciate Professor Li-Chun Wang who has guided me for more than three years. As the lyric goes, I once was lost, but now I am found. I was so unfamiliar with what the true research is, but I have increased some more understanding now.

Secondly, I want to thank all my laboratory members in Mobile Communications and Cloud Computing Laboratory at the Institute of Communications Engineering in National Chiao-Tung University. It is they that provide me so much assistance to finish my research. Especially, Tsung-Ting Chiang spent a lot of his free time helping me solve many problems.

Finally, I owe an enormously debt of gratitude to my parents for their great support these years.

Contents

List of Tables

List of Figures

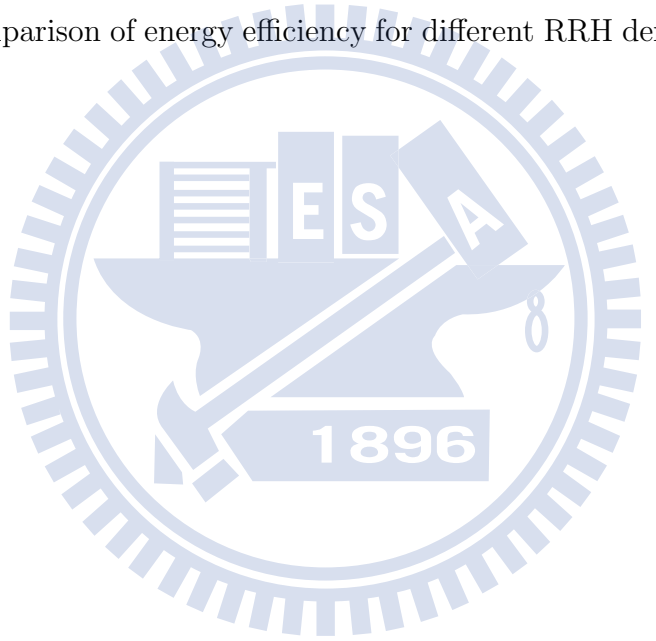

E S A
1896

CHAPTER 1

Introduction

Due to the explosive growth in information and communication traffic as well as demands of better quality of service (QoS) from subscribers, it is estimated that the information and communication technology (ICT) energy consumption is rising at 15-20 percentages per year, in other words, doubling every five years, and such striking increase does not seem to slow down soon. It is reckoned that the ICT industry is responsible for 3 percent of the worldwide annual electrical energy consumption, causing 2-4 percent of world's carbon dioxide emissions [1] [2]. With the increasing awareness of gradual depletion of non-renewable resources and harmful environmental impacts caused by carbon dioxide, it is the social responsibility that cellular network operators should be devoted to develop energy-efficient telecommunication systems. Aside from environmental aspects, the energy cost accounts a great portion of network operators' overall expenditure, and the electric bill is more than $10 billion dollars per year [3]. At present, almost 80 percentages of electrical power for system operation is attributed to radio access network (RAN) [4]. Therefore, efficient transmission schemes and network architectures benefit not only ecological but also economical aspects. Such improvements can be fulfilled in two ways: optimizing base stations (BSs) via more efficient and traffic load adaptive modules, and innovating radio access point deployment strategies as well as transmission technologies to lower the energy consumption and achieve the required system performance.

1.1 Motivation

The traditional network system design mainly focused on spectral efficiency (SE). Energy efficiency (EE) only received little attention, and seldom deemed as a vital performance indicator. As energy-saving issue becomes more crucial, green communication gets more and more important. Therefore, not only SE but also EE should be considered in the system design. There are several techniques to increasing the system throughput. First of all, deploying small cells with macro-cells to build a heterogeneous network (HetNet), which is able to enhance received signal power to guarantee acceptable signal to interference plus noise ratio (SINR). Secondly, higher data rate can be rendered through coordinated multi-point (CoMP) techniques which allow BSs to process signals jointly for mitigating interference [5] [6]. It is true that CoMP and HetNet are promising techniques to improve the system capacity [7]. However, it comes with a price: additional energy consumption. Because increasing BSs needs more power consumption accordingly, and additional backhaul connections among cooperating nodes as well as signal processing power to perform CoMP schemes also need more energy. As mentioned above, both spectral and energy efficiency are vital performance indicators. Hence, the objective of this thesis is to assess spectral and energy efficiency of CoMP transmission in HetNet systems, and to find the appropriate transmission scheme and deployment strategy to achieve energy-efficient transmission.

1.2 Issues

To address the characteristic of the relation between those two performance metrics [8], we consider a point-to-point transmission in additive white Gaussian noise (AWGN) channel. In accordance with Shannon's capacity equation, given the system

bandwidth W and the transmit power P, the maximal reliable transmission rate is

$$R = W\log_2(1 + \frac{P}{WN_0}), \tag{1.1}$$

where N_0 denotes the noise power spectral density. According to SE and EE definitions, SE and EE are

$$\eta_{SE} = \frac{R}{W} = \log_2(1 + \frac{P}{WN_0}), \tag{1.2}$$

and

$$\eta_{EE} = \frac{R}{P} = \frac{W}{P}\log_2(1 + \frac{P}{WN_0}) \tag{1.3}$$

respectively. From (1.2) and (1.3), we can get

$$2^{\eta_{SE}} = 1 + \frac{P}{WN_0}. \tag{1.4}$$

Then, the SE-EE relation can be expressed as

$$\eta_{EE} = \frac{\eta_{SE}}{(2^{\eta_{SE}} - 1)N_0}, \tag{1.5}$$

which is plotted in Fig. 1.1. From (1.5), as η_{EE} approaches to zero, η_{SE} tends to infinity. In contrast, when η_{EE} approaches to zero, η_{SE} converges to $1/(N_0 \ln 2)$. It is impossible to satisfy both metrics in the same time.

However, (1.5) is specific to point to point instead of networks transmission. If more practical constrains and transmission strategies are taken into consideration, such as transmission techniques, modulation and coding schemes, transmission distances, and resource allocation algorithms, the SE-EE curve will not be as monotonic as shown in Fig 1.1 [9]. Therefore, it is worthy of assessing the SE-EE relation for the future energy-efficient communication system design.

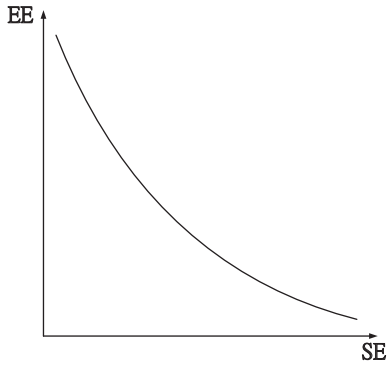

Figure 1.1: The relation between EE and SE.

1.3 Thesis Outline

The remainder of the thesis is organized as follows. In Chapter 2 we introduce the background of our work. System models are illustrated in Chapter 3. In chapter 4, we address our simulation methodology of heterogeneous network CoMP systems. The procedure of our joint design is described in Chapter 5. Then, the numerical and simulation results are shown in Chapter 6. Finally, Chapter 7 concludes the thesis.

CHAPTER 2

Background

2.1 Why Green Communication?

The way people access information has been revolutionized by the consecutively renewing technology. Dramatic growth on data traffic and the requirements for ubiquitous access have triggered tremendous expansion of network infrastructure and correspondingly ascending escalation of energy needs. The estimated growing rate of network subscribers is 20 percent per year, i.e., doubled every five years. It is reckoned that the ICT industry is accountable for three percent of world's annual electrical power consumption and two to four percent of worldwide carbon dioxide emission which put great threats on global environment. There have been shown that about three billion mobile handsets and around three million base sites worldwide. The electricity bill is more than 10 billion dollars each year [10]. From the operators' perspective, reducing energy consumption not only diminishes carbon print, but also saves operating expenditure costs, so the social responsibility and operation profit are both catered. In fact, over 80 percent of the total ICT energy consumption is attributed to the radio access network. Studies have clearly indicated that the power drain of mobile handset equipments is far lower than that of BSs. Hence, energy reduction schemes are supposed to mainly focus on BSs. Such a goal can be achieved by renovating existing network structures with more energy efficient deploy-

ment strategies or applying novel transmission techniques of BSs. Briefly speaking, energy-efficient technologies will be indispensable for helping ICT industries face challenges in a more and more energy-constrained future.

2.2 Coordinated Multi-point Techniques

Cooperation among BSs for data transmissions to one or more user equipment (UE) is known as a key technique to reach the requirement of the IMT-Advance in terms of both overall and cell-edge system throughput of cellular communication networks. The network multiple-input-multiple-output (MIMO) technique is also referred as CoMP by 3GPP. Moreover, it is thought to be one of potential contributors in enhancing energy efficiency of upcoming LTE-A systems. There are four downlink CoMP deployment scenarios [11]:

(1) Scenario 1: Homogeneous network with intra-site CoMP, as shown in Fig. 2.1(a).

(2) Scenario 2: Homogeneous network with high transmit power remote radio heads (RRHs). RRHs are linked to the macro-cell with high speed backhaul, as shown in Fig. 2.1(b).

(3) Scenario 3: Heterogeneous network with low power RRHs within the macro-cell coverage. RRHs share different cell IDs with the macro-cell, as shown in Fig. 2.1(c).

(4) Scenario 4: Heterogeneous network with low power RRHs within the macro-cell coverage. RRHs share the same cell ID with the macro-cell, as shown in Fig. 2.1(c).

Although Scenarios 1 and 2 are developed the earliest, scenario 4 has the most potential and advantages.

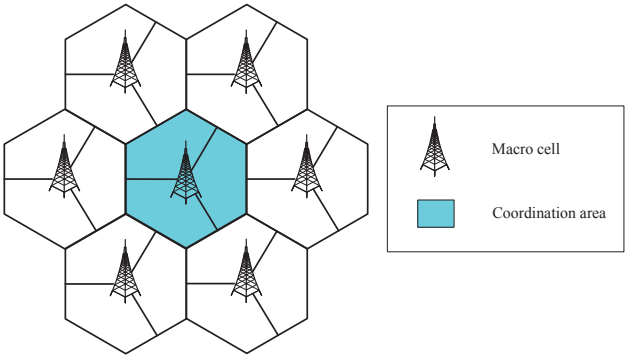

(a) Scenario1.

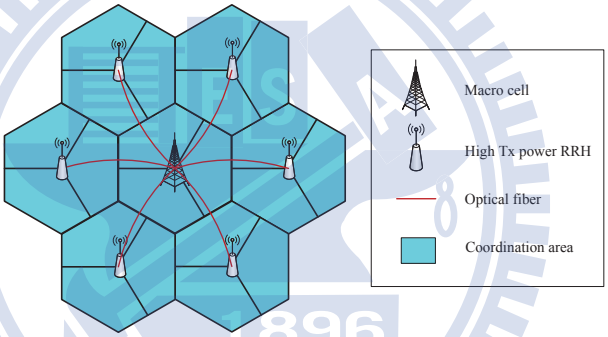

(b) Scenario2.

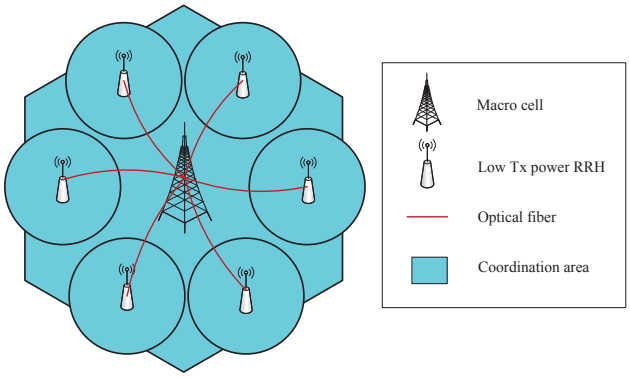

(c) Scenario3/4.

Figure 2.1: Various CoMP scenarios.

In general, CoMP techniques can be categorized into two classes, which are joint processing (JP) and coordinated scheduling / coordinated beamforming (CS/CB). Most of current researches on CoMP schemes have focused on JP. In the class of JP, by sharing channel state information among BSs through network backhaul, the signal can be processed jointly before transmitting and signals from other cells may assist the communication instead of being treated as a detrimental interference. The same information to the target UE is simultaneously transmitted from different cooperating BSs through the same frequency resource and coherently or non-coherently combined at the receiver side, which improves received signal quality and mitigates interferences. In terms of CS/CB, the data to single UE is only available at and transmitted from one point in the cooperating set for a time frequency resource, while user scheduling/beamforming decisions are made among coordinated cells.

2.3 Literature Survey

HetNet is thought to be power efficient for deploying low power nodes to extend the cell coverage and improve system capacity. It is true that SE may increase with the denser network. However, both [12] and [13] indicated that as the number of pico cells exceeds a certain amount, the gain in system throughput cannot compensate the extra power consumption of pico sites, which degrades EE. Hence, small cell deployment is suggested being limited under a certain degree. The work [14] further analyzed HetNet in terms of EE and success probability, indicating that there exists an optimal pico-macro density ratio that maximizes EE, which offers the knowledge in how to establish green heterogeneous networks. [15] pointed out that despite that overall EE is improved, but the macro-cell performance is slightly degraded due to interferences from small cells. In brief, increasing small cells is not always beneficial for improving the system throughput.

Table 2.1: **Comparison of Our Work and Related Works**

	Heterogeneous Networks	**Coordinated Multi-Point**	**System Architecture**	**SE-EE Analysis**
[17]	×	√	√	√
[16]	×	√	√	×
[18]	√	√	×	×
[14]	√	×	√	×
[15]	√	×	√	√
Our Work	√	√	√	√

CoMP techniques can improve network throughput significantly, but it also requires more power to sustain such operations. In [16], authors compared system capacity of various density cooperative networks. Their results shows the denser network is, the SE higher will be. Nevertheless, the relation of energy efficiency is not drawn. Tradeoff between cell throughput gains via inter-site CoMP scheme and increased power dissipation has been investigated under various cell dimensions and cooperation cluster sizes [17]. A similar investigation has been conducted in [18]. The energy efficiency analysis of joint transmission (JT) CoMP in homogeneous and heterogeneous network is addressed. However, both [17] and [18] did not take the concept of cooperation among macro-cell and lower power sites into consideration. We analyze the system capacity and power consumption of heterogeneous CoMP networks under various system settings to seek energy-efficient transmission schemes and system architectures. Related researches are summarized and compared with our work at Table 2.1.

CHAPTER 3

System Models

In this chapter, we illustrate our system models thoroughly. At the beginning, we present the system architecture of our simulator, including the homogeneous network for single user multi-input-multi-output (SU-MIMO) systems and the heterogeneous network for CoMP systems. Channel model and radio environment are introduced in the second section. The power consumption model is given in the last section.

3.1 Cell Layout

3.1.1 Homogeneous Network SU-MIMO System

MIMO transmission techniques have been studied extensively in the past. Spatial multiplexing has drawn much attention due to the capability of increasing spectral efficiency. Spatial multiplexing of multiple data streams to single target UE in the same time-frequency resource is referred as SU-MIMO. We set the homogeneous network SU-MIMO system composed by 19 cells with hexagonal gird as our simulation baseline, which is shown in Fig. 3.1. Each cell is divided into three sectors, and each sector is equipped with a directional antenna.

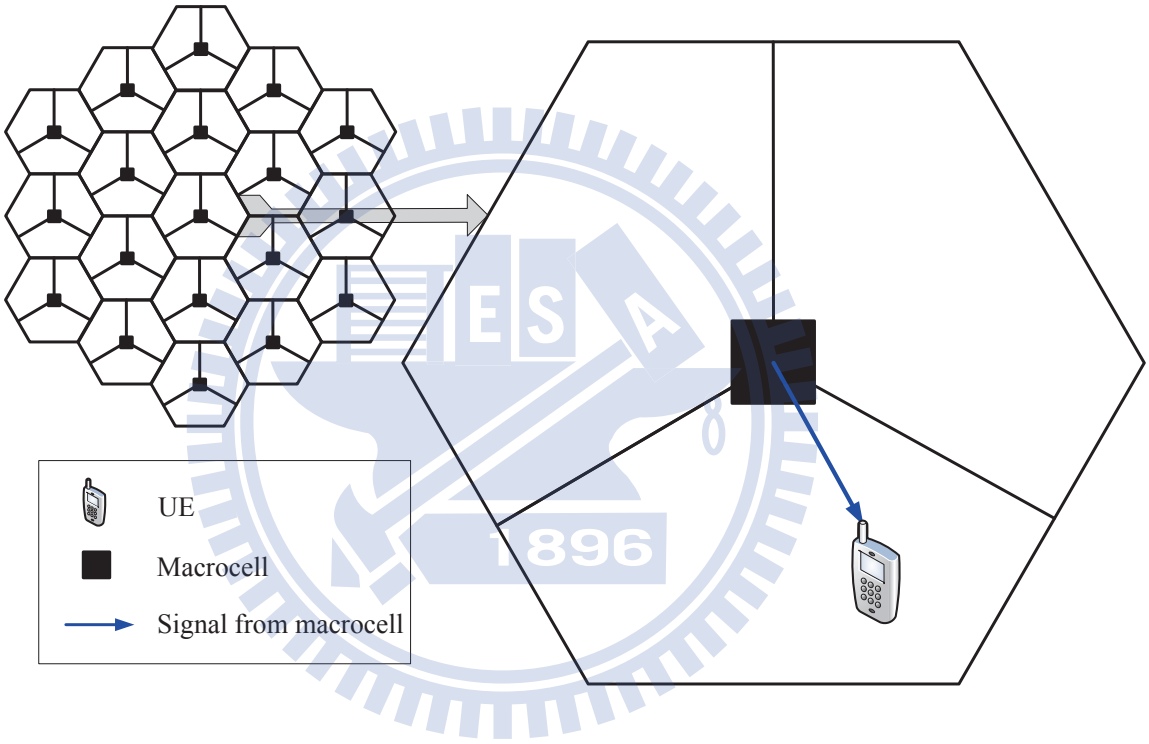

Figure 3.1: Cell architecture of SU-MIMO systems.

3.1.2 Heterogeneous Network CoMP System

In accordance with 3GPP-A Rel-11, downlink CoMP techniques can be categorized into four scenarios, among of which scenario 4 is the most promising. We choose scenario 4 as the simulation environment so as to combine the concepts of HetNet and CoMP techniques. The cellular system is composed of 19 hexagonal cells, where each cell is divided into 3 sectors, and every sector is equipped with directional antennas as shown in Fig. 3.2. The benefit of using directional antenna is that the signal can be concentrated to be transmitted within some range, which makes the signal more strengthened and interferences among sectors can be mitigated. RRHs are deployed in each sector and connected with the macro-cell by 10^9 bytes level optical fibers. Fibers are able to carry a large amount of data. In this way, remote units can exchange information with the macro-cell, and the signal processing can be jointly performed by RRHs and the macro-cell in a centralized manner. Minimum distances between the BS an UE are listed in Table 3.1.

Table 3.1: **Deployment regulations**

	Minimum Distance
Macro-RRH	$> 75m$
RRH-RRH	$> 40m$
Macro-UE	$> 35m$
RRH-UE	$> 10m$

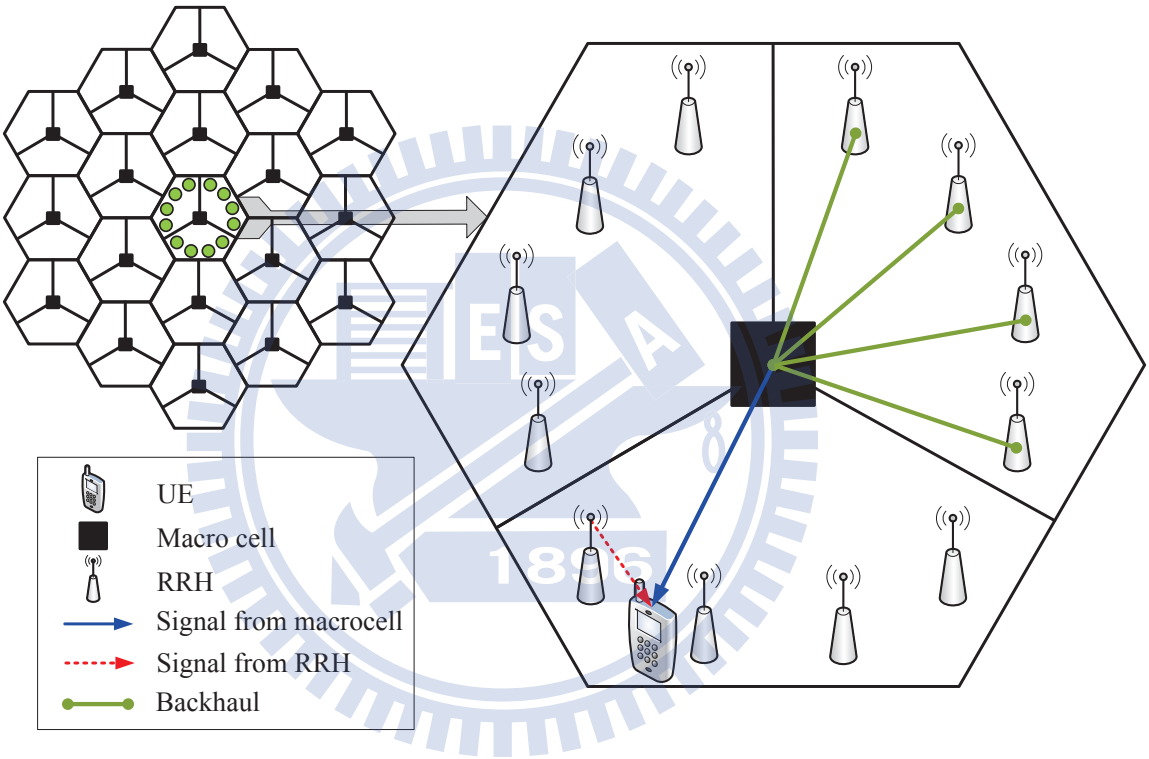

Figure 3.2: Cell architecture of CoMP systems.

3.2 Channel Model

3.2.1 Radio Environment

Based on [19], we consider path loss model, shadowing fading and antenna pattern in the radio environment. The path loss model is a major factor in the analysis and design of the link budget of wireless communication systems, describing how the power density of an electromagnetic wave reduces as it propagates through space. Path loss models of macro-cell and RRH in decibel are defined as:

$$PL_{macro}(d) = 128.1 + 37.6 \cdot \log_{10}(d), \tag{3.1}$$

and

$$PL_{RRH}(d) = 140.7 + 36.7 \cdot \log_{10}(d) \tag{3.2}$$

respectively, where PL_{macro} and PL_{RRH} denote the power attenuation from macro-cell/RRH to UE, and d is the distance between the UE and macro-cell/RRH. Moreover, PL can be further converted into the form of effective gain:

$$G_{PL} = 10^{-(PL(d)/10)}. \tag{3.3}$$

The shadowing fading originates from the obstacles on propagation paths. The distribution is modeled by a log-normal random variable with zero mean. 8 dB standard deviation for macro-cell to UE, and 10 dB standard deviation for RRH to UE, respectively. The horizontal antenna pattern is defined as:

$$A_H(\varphi) = -\min[12(\frac{\varphi}{\varphi_{3dB}})^2, A_m], \tag{3.4}$$

where φ denotes the horizontal angle between BS and UE, φ_{3dB} is 70 degree, and A_m is 25 dB. It can also be written as the form of effective gain:

$$G_{AP}(\varphi) = 10^{[A_H(\varphi)/10]}. \tag{3.5}$$

3.2.2 Sptial Channel Model

The Spatial channel model (SCM) is a standardized model developed by 3GPP for evaluating cellular MIMO systems. In our work, we adopt SCM urban scenario [20]. Assume that there are N resolvable paths in each link from a BS to a UE, and each path consists of M irresolvable subpaths. A simplified plot of SCM is shown in Fig. 3.3.

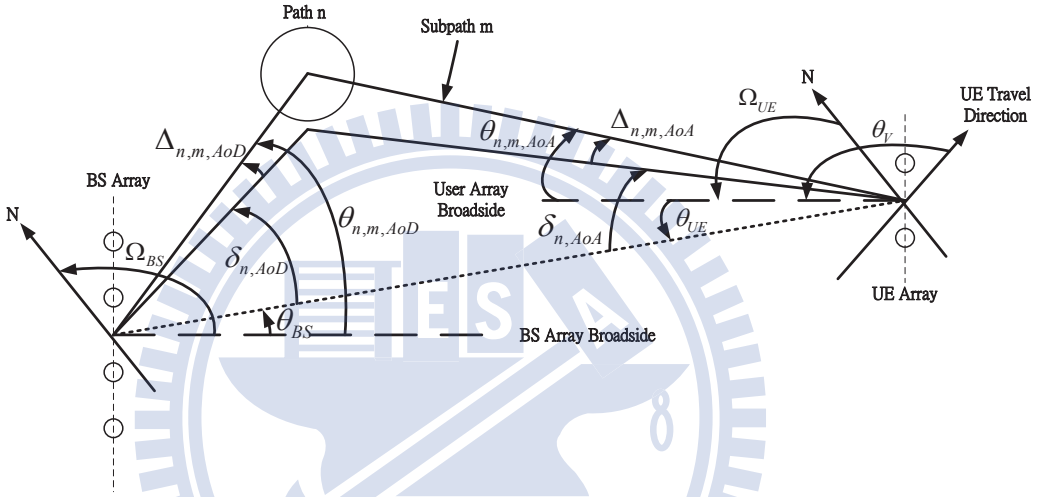

Figure 3.3: Parameters of 3GPP SCM.

For N_t transmit antennas at the BS and N_r receive antennas at the UE, the channel impulse response in time domain for the n_{th} path between the s_{th} transmit and u_{th} receive antenna can be written as:

$$\mathbf{h}_n(t) = \begin{bmatrix} h_{1,1,n}(t) & h_{1,2,n}(t) & \cdots & h_{1,N_t-1,n}(t) & h_{1,N_t,n}(t) \\ h_{2,1,n}(t) & h_{2,2,n}(t) & \cdots & h_{2,N_t-1,n}(t) & h_{2,N_t,n}(t) \\ \vdots & \vdots & \cdots & \vdots & \vdots \\ h_{N_r-1,1,n}(t) & h_{N_r-1,2,n}(t) & \cdots & \vdots & \vdots \\ h_{N_r,1,n}(t) & h_{N_r,2,n}(t) & \cdots & h_{N_r,N_t-1,n}(t) & h_{N_r,N_t,n}(t) \end{bmatrix}. \quad (3.6)$$

Each element in $\mathbf{h}_n(t)$ can be written as:

$$h_{u,s,n}(t) = \sqrt{\frac{P_n}{M}} \sum_{m=1}^{M} [e^{jkd_s \sin(\theta_{n,m,AoD}+\psi_{n,m})} e^{jkd_u \sin(\theta_{n,m,AoA})} e^{jkV \cos(\theta_{n,m,AoA}-\theta_V)t}]. \quad (3.7)$$

where P_n is the power of the n_{th} path, M is the number of subpaths per path, k is the carrier wave number which equals to $2\pi/\lambda$, λ is the carrier wavelength in meters, d_s is the distance in meters from the first antenna to the s_{th} antenna at the BS, $\theta_{n,m,AoD}$ is the angle between the m_{th} subpath of the n_{th} path and the BS array broadside, $\psi_{n,m}$ is the phase of the m_{th} subpath of the n_{th} path which uniformly distributes in the interval $[0°, 360°]$, d_u is the distance in meters from the first antenna to the u_{th} antenna at the UE, $\theta_{n,m,AoA}$ is the angle between the m_{th} subpath of the n_{th} path and the UE array broadside, V is the UE velocity, and θ_V is the angle between the UE travel direction and the UE array broadside. For multi-carrier OFDM systems, the channel impulse response from the s_{th} transmit to the u_{th} receive antenna in frequency domain of the k_{th} subcarrier is:

$$\mathbf{H}_{SCM}(k) = \begin{bmatrix} H_{1,1}(k) & H_{1,2}(k) & \cdots & H_{1,N_t-1}(k) & H_{1,N_t}(k) \\ H_{2,1}(k) & H_{2,2}(k) & \cdots & H_{2,N_t-1}(k) & H_{2,N_t}(k) \\ \vdots & \vdots & \cdots & \vdots & \vdots \\ H_{N_r-1,1}(k) & H_{N_r-1,2}(k) & \cdots & \vdots & \vdots \\ H_{N_r,1}(k) & H_{N_r,2}(k) & \cdots & H_{N_r,N_t-1}(k) & H_{N_r,N_t}(k) \end{bmatrix}. \quad (3.8)$$

Each element in $\mathbf{H}_{SCM}(k)$ can be expressed as:

$$H_{u,s}(k) = FFT\{[h_{u,s,1}(t), h_{u,s,2}(t), ..., h_{u,s,n}(t)]\}, \quad (3.9)$$

where $FFT\{\cdot\}$ denotes the Fourier transform function.

3.3 Power Consumption Model Description

3.3.1 Network Power Consumption

The total network input power includes power consumption in RAN, backhaul, and signal processing for CoMP:

$$P_{total} = P_{site} + P_{sp} + P_{bh}, \tag{3.10}$$

where

$$P_{site} = P_{PDS} + P_{AC} + P_{Trans} + P_{BS}. \tag{3.11}$$

Related details of P_{site} are listed in Table 3.2 [21]. P_{sp} denotes the signal processing power for cooperation, it can be expressed as [17]:

$$P_{sp} = 58 \cdot (0.87 + 0.1 \cdot N_c + 0.03 \cdot N_c^2), \tag{3.12}$$

where N_c denotes the number of cooperated sites. P_{bh} is the power for backhaul connection, which can be written as:

$$P_{bh} = \frac{R}{100M} \cdot 50, \tag{3.13}$$

where R denotes the data rate.

Table 3.2: **Components of the site power**

	$Watt$
P_{PDS}	485.23
P_{AC}	1940.96
P_{Trans}	650

3.3.2 Base Station Power Consumption

There are different types of BS such as macro-cell, micro-cell, pico-cell, femto-cell, and RRH. Because each kind of BS has different constituents and power figures, it is not easy to describe the precise BS architectures and corresponding power dissipation models thoroughly. In our work, we adopt the power consumption model of the baseband unit (BBU) plus remote radio unit (RRU) based BS as illustrated in Fig. 3.4 [22]. The basic idea of BBU plus RRU system is to separate the baseband part and the radio frequency part of BSs. RRUs are connected to the BBU with optical fibers, and each RRU is equipped with transceivers. The BBU is responsible for baseband signal processing and radio resource management, so the signal can be processed jointly at BBUs. It is cost-saving for radio access points deployment because smaller BBUs require less equipment room, and RRUs can be deployed more flexibly depends on traffic needs.

Each BS consists of multiple transceivers (TRXs), and each TRX is comprised of a power amplifier (PA), a radio frequency (RF) module, a baseband processor, a DC-DC supply, and an AC-DC unit (mains supply), which is shown in Fig. 3.5. As a result, we can decompose the power consumption model into four classes generally [23] [24] :

(1) Power Amplifier (PA): In this part, we consider the PA power efficiency and feeder losses which is caused by extra feedback for pre-distortion and additional signal processing. For small cells, feeder losses are elided, but necessary in macro and micro cells. The power consumption of a PA can be written as:

$$P_{PA} = \frac{P_{out}}{\eta_{PA}(1 - \sigma_{feed})}, \tag{3.14}$$

where η_{PA} is the PA efficiency, and σ_{feed} is the feeder loss factor.

(2) Radio Frequency (RF): The RF part contains a transmitter and a receiver for

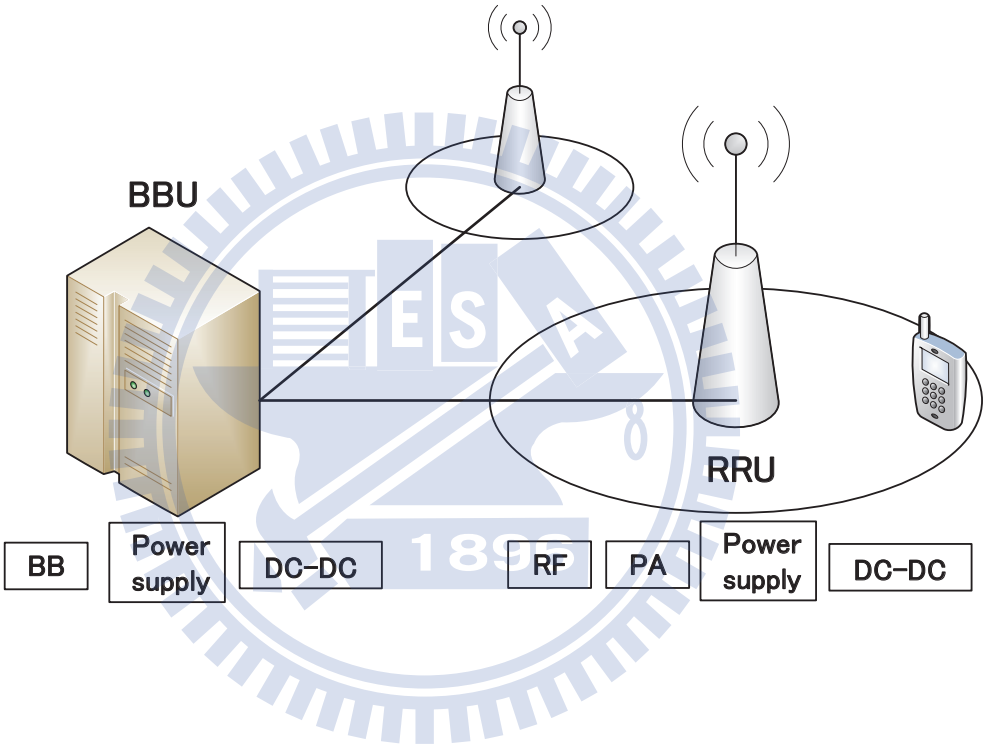

Figure 3.4: BBU+RRU based system.

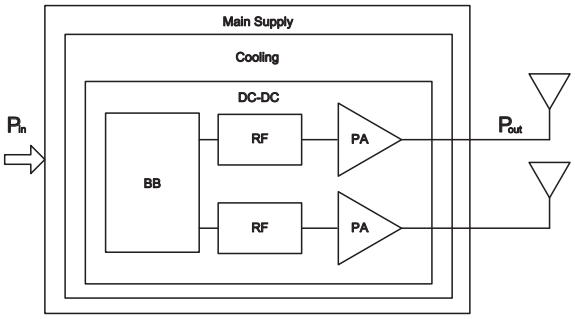

Figure 3.5: Power model of a BS.

downlink and uplink, respectively. Different types of RF modules are required for different types of BSs. For example, low-intermediate frequency (IF) are suitable for macro and micro sites, and zero-IF is favored by smaller cells.

(3) Baseband unit: The baseband unit deals with modulation/demodulation, channel coding/decoding, channel estimation, equalization, pre-distortion, etc.

(4) Heat emission: Any losses related to the system powering are included in this category, such as DC-DC conversion and mains supply.

According to above, given PA, RF, and baseband unit power consumption, P_{PA}, P_{RF} and P_{BB}, the power consumption for BS input is:

$$P_{BS} = \beta[N_{TRX}(P_{PA} + P_{RF} + P_{BB})], \tag{3.15}$$

where β is defined as:

$$\beta = \frac{1}{(1-\sigma_{DC})(1-\sigma_{MS})}, \tag{3.16}$$

and σ_{DC}, σ_{MS},and σ_{cool} are loss factors of the DC/DC, mains supply and cooling system. Thus, the input power for BS can be further expressed as:

$$P_{BS} = N_{TRX} \cdot \frac{\frac{P_{\max}}{\eta_{PA}} + P_{RF} + P_{BB}}{(1-\sigma_{DC})(1-\sigma_{MS})}. \tag{3.17}$$

We assume that the BS power consumption is proportional to the number of transceiver chains N_{TRX}, namely, transmit/receive antenna pairs per site, and all the BSs with the maximal load,

$$P_{\max} = 10^{(P_{out}+\sigma_{feed}-30)/10}. \tag{3.18}$$

The related power consumption parameters of different types BSs are listed in Table 3.3.

Table 3.3: **Power consumption for various BSs**

			Macro BBU	**Macro RRU**	**Pico BBU**	**Pico RRU**
PA	P_{out}	[W]	0	46	0	30
	σ_{feeder}	[dBm]	0	1	0	0
	P_{max}	[W]	0	50.11	0	1
	η_{PA}	[%]	0	31.1	0	6.7
	P_{PA}	[W]	0	161.15	0	14.92
Heat emission	σ_{DC}	[%]	8	8	9	9
	σ_{MS}	[%]	9	9	12	12
	β	#	1.19	1.19	1.24	1.24
RF	P_{RF}	[W]	0	12.9	0	1
BB	P_{BB}	[W]	29.6	0	3	0
	Sectors	#	3	1	1	1
	Antennas	#	2	2	1	1
	Carriers	#	1	1	1	1
	P_{in}	[W]	212.13	415.79	3.74	19.88

CHAPTER 4

Heterogeneous CoMP Networks Simulator

In this chapter, the simulation environment of the 3GPP LTE-A heterogeneous coordination multi-point networks will be illustrated in details, including joint signal process for base station cooperation, precoding method, scheduling method, and SINR calculation.

4.1 Codebook-based Precoding

In FDD systems, the CSI needs to be fed back from UEs to the eNB. It is well known that the system performance can be improved with full channel state information (CSI) at the transmitter. However, because the feedback channel bandwidth is limited, complete channel state feedback leads to excessive overhead. Therefore, the codebook-based precoding method is adopted to reduce the feedback overhead. The UE calculates the precoding matrix and feedback a precoding matrix indicator (PMI) as the index of a codeword. The codebook is designed in the off-line manner, and the same codebook set is available at both the transmitter and the receiver. The feedback overhead can be reduced enormously by only feeding the PMI back rather than the full precoding matrix.

Codebooks for two antenna and four transmit antenna ports are defined in [25]. Tables 4.1 and 4.2 list codewords for two and four transmit antenna ports, respectively. The Frobenius norm of each codeword is normalized to unity to remain the same

transmit power.

Table 4.1: **Codebook for Two Antenna Ports**

Index	**Rank-1**	**Rank-2**
$\mathbf{C}_0$	$\frac{1}{\sqrt{2}}\begin{bmatrix}1\\1\end{bmatrix}$	$\frac{1}{2}\begin{bmatrix}1 & 1\\1 & -1\end{bmatrix}$
$\mathbf{C}_1$	$\frac{1}{\sqrt{2}}\begin{bmatrix}1\\-1\end{bmatrix}$	$\frac{1}{2}\begin{bmatrix}1 & 1\\j & -j\end{bmatrix}$
$\mathbf{C}_2$	$\frac{1}{\sqrt{2}}\begin{bmatrix}1\\j\end{bmatrix}$	
$\mathbf{C}_3$	$\frac{1}{\sqrt{2}}\begin{bmatrix}1\\-j\end{bmatrix}$	

For four transmit antennas, the householder matrix $\mathbf{W}_c$ can be derived by $\mathbf{u}_c$, i.e., $\mathbf{W}_c = \mathbf{I}_4 - 2\mathbf{u}_c\mathbf{u}_c^H/\mathbf{u}_c^H\mathbf{u}_c$. $\mathbf{W}_c^a$ denotes the a_{th} column vector of $\mathbf{W}_c$, and $\mathbf{W}_c^{a,b}$ denotes a_{th} and b_{th} column vectors of $\mathbf{W}_c$.

We assume that UEs can estimate the CSI perfectly based on reference signals from BSs. Singular value decomposition-based (SVD) precoding method is adopted in our work. Denote $\mathbf{H}_{m,n,i}$ as the channel matrix from the m_{th} sector to the i_{th} UE in the n_{th} sector. Then, the channel matrix is decomposed by the SVD technique:

$$\mathbf{H}_{m,n,i} = \mathbf{U}_{m,n,i}\mathbf{D}_{m,n,i}\mathbf{V}_{m,n,i}^H, \tag{4.1}$$

where

$$\mathbf{U}_{m,n,i} = [\mathbf{u}_{m,n,i}^1 \cdots\cdots \mathbf{u}_{m,n,i}^{N_r}] \in C^{N_r \times N_r}, \tag{4.2}$$

Table 4.2: **Codebook for Four Antenna Ports**

Index	$\mathbf{u}_c$	**Rank-1**	**Rank-2**
$\mathbf{C}_0$	$\mathbf{u}_0 = \begin{bmatrix} 1 & -1 & -1 & -1 \end{bmatrix}^{\mathrm{T}}$	$\mathbf{W}_0^1$	$\mathbf{W}_0^{1,4}/\sqrt{2}$
$\mathbf{C}_1$	$\mathbf{u}_1 = \begin{bmatrix} 1 & -j & 1 & j \end{bmatrix}^{\mathrm{T}}$	$\mathbf{W}_1^1$	$\mathbf{W}_1^{1,4}/\sqrt{2}$
$\mathbf{C}_2$	$\mathbf{u}_2 = \begin{bmatrix} 1 & 1 & -1 & 1 \end{bmatrix}^{\mathrm{T}}$	$\mathbf{W}_2^1$	$\mathbf{W}_2^{1,4}/\sqrt{2}$
$\mathbf{C}_3$	$\mathbf{u}_3 = \begin{bmatrix} 1 & j & 1 & -j \end{bmatrix}^{\mathrm{T}}$	$\mathbf{W}_3^1$	$\mathbf{W}_3^{1,2}/\sqrt{2}$
$\mathbf{C}_4$	$\mathbf{u}_4 = \begin{bmatrix} 1 & (-1-j)/\sqrt{2} & -j & (1-j)/\sqrt{2} \end{bmatrix}^{\mathrm{T}}$	$\mathbf{W}_4^1$	$\mathbf{W}_4^{1,4}/\sqrt{2}$
$\mathbf{C}_5$	$\mathbf{u}_5 = \begin{bmatrix} 1 & (1-j)/\sqrt{2} & j & (1-j)/\sqrt{2} \end{bmatrix}^{\mathrm{T}}$	$\mathbf{W}_5^1$	$\mathbf{W}_5^{1,4}/\sqrt{2}$
$\mathbf{C}_6$	$\mathbf{u}_6 = \begin{bmatrix} 1 & (1+j)/\sqrt{2} & -j & (-1+j)/\sqrt{2} \end{bmatrix}^{\mathrm{T}}$	$\mathbf{W}_6^1$	$\mathbf{W}_6^{1,3}/\sqrt{2}$
$\mathbf{C}_7$	$\mathbf{u}_7 = \begin{bmatrix} 1 & (-1+j)/\sqrt{2} & j & (1+j)/\sqrt{2} \end{bmatrix}^{\mathrm{T}}$	$\mathbf{W}_7^1$	$\mathbf{W}_7^{1,3}/\sqrt{2}$
$\mathbf{C}_8$	$\mathbf{u}_8 = \begin{bmatrix} 1 & -1 & 1 & 1 \end{bmatrix}^{\mathrm{T}}$	$\mathbf{W}_8^1$	$\mathbf{W}_8^{1,2}/\sqrt{2}$
$\mathbf{C}_9$	$\mathbf{u}_9 = \begin{bmatrix} 1 & -j & -1 & -j \end{bmatrix}^{\mathrm{T}}$	$\mathbf{W}_9^1$	$\mathbf{W}_9^{1,4}/\sqrt{2}$
$\mathbf{C}_{10}$	$\mathbf{u}_{10} = \begin{bmatrix} 1 & 1 & 1 & -1 \end{bmatrix}^{\mathrm{T}}$	$\mathbf{W}_{10}^1$	$\mathbf{W}_{10}^{1,3}/\sqrt{2}$
$\mathbf{C}_{11}$	$\mathbf{u}_{11} = \begin{bmatrix} 1 & j & -1 & j \end{bmatrix}^{\mathrm{T}}$	$\mathbf{W}_{11}^1$	$\mathbf{W}_{11}^{1,3}/\sqrt{2}$
$\mathbf{C}_{12}$	$\mathbf{u}_{12} = \begin{bmatrix} 1 & -1 & -1 & 1 \end{bmatrix}^{\mathrm{T}}$	$\mathbf{W}_{12}^1$	$\mathbf{W}_{12}^{1,2}/\sqrt{2}$
$\mathbf{C}_{13}$	$\mathbf{u}_{13} = \begin{bmatrix} 1 & -1 & 1 & 1- \end{bmatrix}^{\mathrm{T}}$	$\mathbf{W}_{13}^1$	$\mathbf{W}_{13}^{1,3}/\sqrt{2}$
$\mathbf{C}_{14}$	$\mathbf{u}_{14} = \begin{bmatrix} 1 & 1 & -1 & -1 \end{bmatrix}^{\mathrm{T}}$	$\mathbf{W}_{14}^1$	$\mathbf{W}_{14}^{1,3}/\sqrt{2}$
$\mathbf{C}_{15}$	$\mathbf{u}_{15} = \begin{bmatrix} 1 & 1 & 1 & 1 \end{bmatrix}^{\mathrm{T}}$	$\mathbf{W}_{15}^1$	$\mathbf{W}_{15}^{1,2}/\sqrt{2}$

$$\mathbf{D}_{m,n,i} = \begin{bmatrix} \lambda^1_{m,n,i} & 0 & \cdots & \cdots & 0 & 0 & \cdots & 0 \\ 0 & \ddots & 0 & 0 & \vdots & \vdots & \ddots & \vdots \\ \vdots & 0 & \ddots & 0 & \vdots & \vdots & \ddots & \vdots \\ \vdots & 0 & 0 & \ddots & 0 & \vdots & \ddots & \vdots \\ 0 & \cdots & \cdots & 0 & \lambda^{N_r}_{m,n,i} & 0 & \cdots & 0 \end{bmatrix} \in R^{N_r \times N_t}, \tag{4.3}$$

and

$$\mathbf{V}^H_{m,n,i} = [\mathbf{v}^1_{m,n,i} \cdots\cdots \mathbf{v}^{N_t}_{m,n,i}]^H \in C^{N_t \times N_t}. \tag{4.4}$$

Note that $\lambda^1_{m,n,i} \geq \lambda^2_{m,n,i} \geq ... \geq \lambda^{N_r}_{m,n,i}$. For SVD-based precoding techniques, $\mathbf{V}_{m,n,i}$ is exploited, and each column of $\mathbf{V}_{m,n,i}$ is called an Eigenvector of $\mathbf{H}_{m,n,i}(\mathbf{H}_{m,n,i})^H$, which is related to an Eigenmode of the channel. The individual Eigenmode quality can be defined by each singular value of $\mathbf{H}_{m,n,i}$. If the signal is transmitted with N_D data streams to the i_{th} UE in the n_{th} sector, N_D column vectors from the left of $\mathbf{V}_{m,n,i}$ will be selected as the full precoding matrix $\widetilde{\mathbf{W}}_{m,n,i}$. The corresponding codeword is selected based on the minimum angle between each codeword and the full precoding matrix:

$$a = \arg\max_i trace\left(\left|\mathbf{C}^H_i \widetilde{\mathbf{W}}_{m,n,i}\right|\right) , \tag{4.5}$$

where $\mathbf{C}_i$ denotes the codeword defined in Tables 4.1 and 4.2, and a is the PMI to be fed back to BSs.

4.2 Transmission Equations

For the sake of simplicity, we discuss the following equations in the single carrier case. The OFDM multi-carrier case can be extended in the same way. Let $\mathbf{H}_{m,n,i} \in C^{N_r \times N_t}$ represent the channel matrix from the m_{th} sector to the i_{th} UE in the n_{th} sector, and

$\mathbf{H}^{RRH}_{m_r,n,i} \in C^{N_r \times N_t}$ denotes the channel matrix from the r_{th} RRH in the m_{th} sector to the i_{th} UE in the n_{th} sector similarly. In accordance with (3.3), (3.5), and (3.9), the channel matrix $\mathbf{H}_{m,n,i}$ can be written as:

$$\mathbf{H}_{m,n,i} = \mathbf{H}_{SCM}\sqrt{G_{PL} \cdot \sigma_S \cdot G_{AP}}, \tag{4.6}$$

where σ_S is the shadowing factor. In the same manner, $\mathbf{H}^{RRH}_{m_r,n,i}$ has a similar mathematic form with $\mathbf{H}_{m,n,i}$. For SU-MIMO transmission, the effective channel matrix $\mathbf{H}^{eff}_{m,n,i} \in C^{N_r \times N_t}$ detected by the i_{th} UE is

$$\mathbf{H}^{eff}_{m,n,i} = \mathbf{H}_{m,n,i}. \tag{4.7}$$

As for CoMP transmission, RRHs share the same cell ID with the macro-cell, the whole network can be regarded as a distributed antenna system. Thus data transmitted by the macro-cell and RRHs are placed on the same resource blocks (RBs). Consequently, the effective channel matrix $\mathbf{H}^{eff}_{m,n,i} \in C^{N_r \times N_t}$ detected by the i_{th} UE in the n_{th} sector is the combination of channel matrices from the macro-cell and RRHs, which can be written as:

$$\mathbf{H}^{eff}_{m,n,i} = \sum_{m} \mathbf{H}_{m,n,i} + \sum_{r} \mathbf{H}^{RRH}_{m_r,n,i}. \tag{4.8}$$

4.2.1 Single UE Case

Assume that the n_{th} sector is the serving sector antenna of the i_{th} UE. The received signal matrix of the i_{th} UE in the n_{th} sector can be written as:

$$\mathbf{Y}_{n,n,i} = \overbrace{\mathbf{H}^{eff}_{n,n,i}\mathbf{W}_{n,n,i}\mathbf{X}_{n,n,i}}^{\text{Desired signal}} + \overbrace{\sum_{m \neq n}^{57} \mathbf{H}^{eff}_{m,n,i}\mathbf{W}_{m,m,i}\mathbf{X}_{m,m,i}}^{\text{Inter-cell interference}} + \overbrace{\mathbf{N}_{n,n,i}}^{Noise}. \tag{4.9}$$

The second term in (4.9) is the interference from other sectors. Thus $\mathbf{X}_{n,n,i}$ is the desired data matrix to the i_{th} UE in the n_{th} sector, $\mathbf{W}_{n,n,i}$ is the precoding matrix to

the i_{th} UE in the n_{th} sector, and $\mathbf{N}_{n,n,i} \in C^{N_r \times 1}$ is the additive white Gaussian noise with power spectral density $\sigma_n^2 = -174$dBm/Hz.

For the rank-1 transmission, the maximal ratio combining (MRC) technique is adopted. Assume that the desired data matrix is $\mathbf{X}_{n,n,i} = x^1_{n,n,i}$ and the corresponding precoding matrix is $\mathbf{W}_{n,n,i} = \mathbf{w}^1_{n,n,i}$. The desired data can be demodulated via multiplying $\mathbf{Y}_{n,n,i}$ by the MRC matrix:

$$\mathbf{M}_{n,n,i} = [\mathbf{H}^{eff}_{n,n,i}\mathbf{W}_{n,n,i}]^H. \tag{4.10}$$

For the rank-2 transmission, the minimum mean square error (MMSE) receive technique is adopted. Assume that the desired data matrix is $\mathbf{X}_{n,n,i} = \begin{bmatrix} x^1_{n,n,i} & x^2_{n,n,i} \end{bmatrix}$ and the corresponding precoding matrix is $\mathbf{W}_{n,n,i} = \begin{bmatrix} \mathbf{w}^1_{n,n,i} & \mathbf{w}^2_{n,n,i} \end{bmatrix}$. The desired data can be demodulated via multiplying $\mathbf{Y}_{n,n,i}$ by MMSE matrices $\mathbf{M}^1_{n,n,i} \in \mathcal{C}^{1\times N_r}$ and $\mathbf{M}^2_{n,n,i} \in \mathcal{C}^{1\times N_r}$, respectively, where

$$\mathbf{M}^1_{n,n,i} = \left[\left(\sigma_n^2\mathbf{I} + \mathbf{H}_{n,n,i}\mathbf{w}^2_{n,n,i}\left(\mathbf{H}_{n,n,i}\mathbf{w}^2_{n,n,i}\right)^H\right)^{-1}\mathbf{H}_{n,n,i}\mathbf{w}^1_{n,n,i}\right]^H, \tag{4.11}$$

and

$$\mathbf{M}^2_{n,n,i} = \left[\left(\sigma_n^2\mathbf{I} + \mathbf{H}_{n,n,i}\mathbf{w}^1_{n,n,i}\left(\mathbf{H}_{n,n,i}\mathbf{w}^1_{n,n,i}\right)^H\right)^{-1}\mathbf{H}_{n,n,i}\mathbf{w}^2_{n,n,i}\right]^H. \tag{4.12}$$

Hence, the received SINR of the i_{th} UE in the n_{th} sector can be written as:

$$\gamma_{n,n,i} = \frac{P_{Tx}\left\|\mathbf{M}_{n,n,i}\mathbf{H}^{eff}_{n,n,i}\mathbf{W}_{n,n,i}\mathbf{X}_{n,n,i}\right\|^2}{P_{Tx}\left\|\mathbf{M}_{n,n,i}\sum_{m\neq n}^{57}\mathbf{H}^{eff}_{m,n,i}\mathbf{W}_{m,m,i}\mathbf{X}_{m,m,i}\right\|^2 + \left\|\mathbf{M}_{n,n,i}\mathbf{N}_{n,n,i}\right\|^2}, \tag{4.13}$$

where P_{Tx} is the transmit power of BS.

4.2.2 Multiple UE Case

We assume that there are two UEs in each sector: the i_{th} UE and the j_{th} UE. The received signal matrix of the i_{th} UE in the n_{th} sector can be written as:

$$\mathbf{Y}_{n,n,i} = \overbrace{\mathbf{H}^{eff}_{n,n,i}\mathbf{W}_{n,n,i}\mathbf{X}_{n,n,i}}^{\text{Desired signal}} + \overbrace{\mathbf{H}^{eff}_{n,n,j}\mathbf{W}_{n,n,j}\mathbf{X}_{n,n,j}}^{\text{Inter-user interference}} + \overbrace{\sum_{m\neq n}^{57}(\mathbf{H}^{eff}_{m,n,i}\mathbf{W}_{m,m,i}\mathbf{X}_{m,m,i} + \mathbf{H}^{eff}_{m,n,j}\mathbf{W}_{m,m,j}\mathbf{X}_{m,m,j})}^{\text{Inter-cell interference}} + \overbrace{\mathbf{N}_{n,n,i}}^{\text{Noise}} . \tag{4.14}$$

The second term of (4.14) is the interference from the other UE in the same cell, and the third term is the interference from other cells. Likewise, we can derive the received signal matrix of the j_{th} UE in the n_{th} sector like (4.14) in the same manner:

$$\mathbf{Y}_{n,n,j} = \overbrace{\mathbf{H}^{eff}_{n,n,j}\mathbf{W}_{n,n,j}\mathbf{X}_{n,n,j}}^{\text{Desired signal}} + \overbrace{\mathbf{H}^{eff}_{n,n,i}\mathbf{W}_{n,n,i}\mathbf{X}_{n,n,i}}^{\text{Inter-user interference}} + \overbrace{\sum_{m\neq n}^{57}(\mathbf{H}^{eff}_{m,n,j}\mathbf{W}_{m,m,j}\mathbf{X}_{m,m,j} + \mathbf{H}^{eff}_{m,n,i}\mathbf{W}_{m,m,i}\mathbf{X}_{m,m,i})}^{\text{Inter-cell interference}} + \overbrace{\mathbf{N}_{n,n,j}}^{\text{Noise}} . \tag{4.15}$$

To demodulate received signals of the i_{th} and the j_{th} UE, we multiply $\mathbf{Y}_{n,n,i}$ and $\mathbf{Y}_{n,n,j}$ by MMSE matrix

$$\mathbf{M}^1_{n,n,i} = [({\sigma_n}^2 I + \mathbf{H}^{eff}_{n,n,i}\mathbf{W}_{n,n,j}(\mathbf{H}^{eff}_{n,n,i}\mathbf{W}_{m,m,j})^H)^{-1}\mathbf{H}^{eff}_{n,n,i}\mathbf{W}_{n,n,i}]^H \tag{4.16}$$

and

$$\mathbf{M}^1_{n,n,j} = [({\sigma_n}^2 I + \mathbf{H}^{eff}_{n,n,j}\mathbf{W}_{n,n,i}(\mathbf{H}^{eff}_{n,n,j}\mathbf{W}_{m,m,i})^H)^{-1}\mathbf{H}^{eff}_{n,n,j}\mathbf{W}_{n,n,j}]^H, \tag{4.17}$$

respectively. Hence, the received SINRs of the i_{th} UE and the j_{th} UE in the n_{th} sector can be written as:

$$\gamma_{n,n,i} = \frac{P_{Tx}\left\|\mathbf{M}_{n,n,i}\mathbf{H}^{eff}_{n,n,i}\mathbf{W}_{n,n,i}\mathbf{X}_{n,n,i}\right\|^2}{P_{Tx}\left\|\mathbf{M}_{n,n,i}\sum_{m\neq n}^{57}\mathbf{H}^{eff}_{m,n,i}\mathbf{W}_{m,m,i}\mathbf{X}_{m,m,i}\right\|^2 + \left\|\mathbf{M}_{n,n,i}\mathbf{N}_{n,n,i}\right\|^2}, \tag{4.18}$$

and

$$\gamma_{n,n,j} = \frac{P_{Tx}\left\|\mathbf{M}_{n,n,j}\mathbf{H}^{eff}_{n,n,j}\mathbf{W}_{n,n,j}\mathbf{X}_{n,n,j}\right\|^2}{P_{Tx}\left\|\mathbf{M}_{n,n,j}\sum_{m\neq n}^{57}\mathbf{H}^{eff}_{m,n,j}\mathbf{W}_{m,m,j}\mathbf{X}_{m,m,j}\right\|^2 + \left\|\mathbf{M}_{n,n,j}\mathbf{N}_{n,n,j}\right\|^2}, \tag{4.19}$$

respectively, where P_{Tx} is the transmit power of a BS.

4.3 CoMP Schemes

In the JP transmission, the precoding matrix is decided by decomposing the received effective channel matrix from multiple BSs based on the SVD method. For the intra-site JP, the effective channel matrix of the i_{th} UE in the n_{th} sector can be expressed as

$$\mathbf{H}^{eff}_{m,n,i} = \mathbf{H}_{m,n,i} + \sum_{r}\mathbf{H}^{RRH}_{m_r,n,i}. \tag{4.20}$$

For the inter-site plus intra-site JP, the effective channel matrix of the i_{th} UE in the n_{th} sector can be expressed as

$$\mathbf{H}^{eff}_{m,n,i} = \sum_{m=1}^{3}\mathbf{H}_{m,n,i} + \sum_{r}\mathbf{H}^{RRH}_{m_r,n,i}. \tag{4.21}$$

Apart from JP, we also consider the CS/CB technique for the inter-cell coordination. All the three cells serve an UE in the same time for JP transmission. On the other hand, each cell serves only an UE at a time, but manages to reduce the interference to UEs in other cells for CS/CB transmission . Take a two cell system as shown in Fig. 4.1 for illustration. We can express the received signal of UE1 as

$$\mathbf{Y}_1 = \mathbf{H}_{11}\mathbf{W}_1\mathbf{X}_1 + \mathbf{H}_{21}\mathbf{W}_2\mathbf{X}_2 + \mathbf{N}, \tag{4.22}$$

where $\mathbf{H}_{11}$ denotes the channel matrix from BS1 to UE1, $\mathbf{H}_{21}$ denotes the channel matrix from BS2 to UE1. $\mathbf{W}_1$ and $\mathbf{W}_2$ are precoding matrices of UE1 and UE2, respectively. The SINR of UE1 can be written as:

$$SINR_1 = \frac{P_1 \|\mathbf{M}_1\mathbf{H}_{11}\mathbf{W}_1\|^2}{P_2 \|\mathbf{M}_1\mathbf{H}_{21}\mathbf{W}_2\|^2 + {\sigma_n}^2}, \tag{4.23}$$

where $\mathbf{M}$ denotes the demodulation matrix, P is the transmit power, and ${\sigma_n}^2$ denotes the thermal noise power. In order to maximize $SINR_1$, the interference term of (4.23) should be mitigated. Thus, once $\mathbf{W}_1$ is determined, we try to select a $\mathbf{W}_2$ which makes $\mathbf{H}_{21}\mathbf{W}_2$ approaches zero from the codebook, in other words, finding a precoing matrix which tends to be orthogonal to the channel matrix. For the rank-1 transmission, $\mathbf{W}_2$ is chosen from the codebook according to

$$\arg\min_j (|\mathbf{H}_{11}\mathbf{W}_1(\mathbf{H}_{21}\mathbf{W}_j)|^H). \tag{4.24}$$

For the rank-2 transmission, $\mathbf{W}_2$ is chosen from the codebook according to

$$\arg\min_j [tr(|\mathbf{H}_{11}\mathbf{W}_1(\mathbf{H}_{21}\mathbf{W}_j)|^H)]. \tag{4.25}$$

4.4 Proportional Fair Scheduling

Proportional fair scheduling is a compromise-based scheduling algorithm. Both fairness of all UEs and maximizing the network throughput are taken into account. If maximizing network throughput is the highest priority, UEs with better link quality will be always served and UEs with poor link quality will be neglected. With proportional fair scheduling, both transmission rate and fairness are concerned. An UE will be served if its current transmission rate is high or its past average transmission rate is low. On the contrary, if the current transmission rate of another UE is low or its past average transmission rate is high, its serving priority is lower than the former

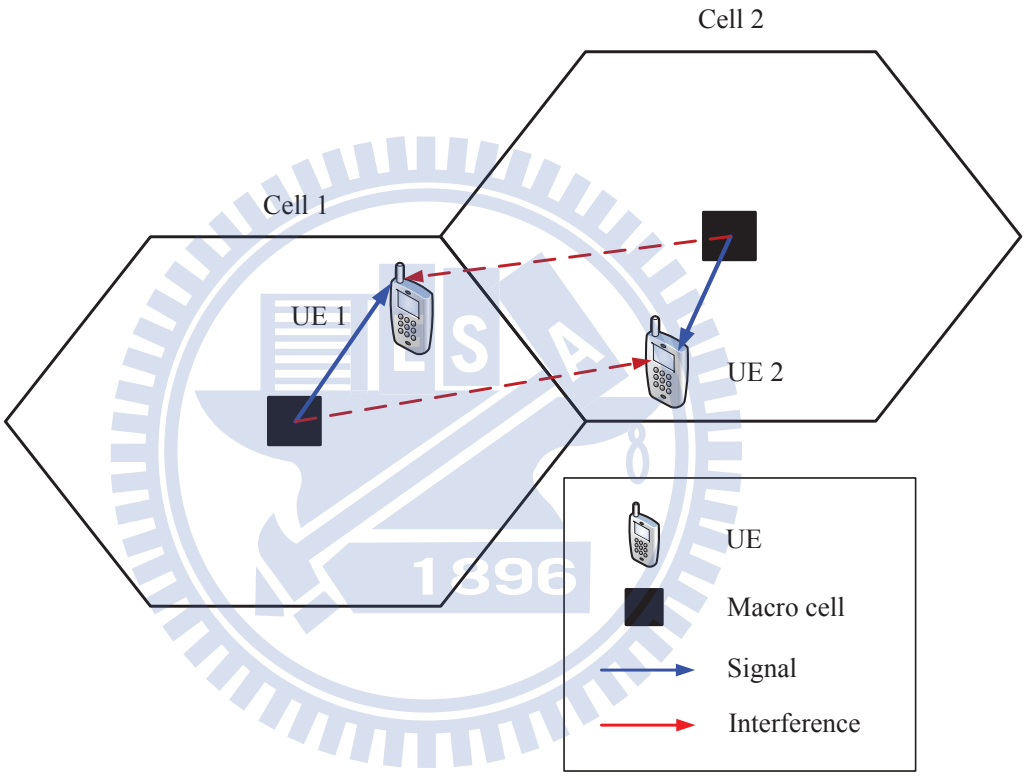

Figure 4.1: Two cell scenario of CS/CB.

one. By using proportional fair scheduling, the BS transmits data to the UE i^* in the r_{th} RB:

$$i^* = \arg\max_i \frac{R_i}{T_i}, \tag{4.26}$$

where $i = 1, 2, ..., N$, R_i represents the current transmission rate of the i_{th} UE in the r_{th} RB, and T_i denotes the past average transmission rate of the i_{th} UE before the r_{th} RB.

4.5 Exponential Effective SINR Mapping (EESM)

Exponential Effective SINR Mapping (EESM) method is used to map the instantaneous subcarrier channel state, such as instantaneous SINR, to the corresponding BLER (Block Error Rate) value. EESM maps a set of subcarriers' SINRs into an instantaneous effective SINR. The generalized EESM is stated as:

$$\gamma_{eff} \equiv EESM(\gamma, \beta) = -\beta \ln(\frac{1}{N_c} \sum_{j=1}^{N_c} e^{-\frac{\gamma_j}{\beta}}), \tag{4.27}$$

where γ_j is the SINR of j_{th} subcarrier and N_c is the number of subcarrier per subband. In the 3GPP Release 9, 15 different modulation and coding schemes (MCS) corresponding to 15 different CQI are defined in [26]. The effective SINR can be mapped to a certain MCS by SINR-BLER curve simulated by link level simulator [27]. We choose the highest MCS with BLER not exceeding 0.1.

4.6 Hybrid Automatic Repeat Request (HARQ)

Since the link level behavior is not included in our system level simulation, we model the transmission error by introducing a random variable with probability mass func-

tion (PMF) [28]:

$$P_e(X) = \begin{cases} 0.1, & x = 0 \\ 0.9, & x = 1 \end{cases}, \tag{4.28}$$

where $x = 0$ represents the occurred error, and $x = 1$ represents the successful transmission. If there is an error, data will be retransmitted again in the next transmission time interval (TTI). Suppose that we obtain a throughput T before considering retransmission. Then, the relation between retransmission time N_{re} which is not exceeding three and throughput T_{re} is:

$$T_{re} = \frac{T}{(1 + N_{re})}, \tag{4.29}$$

where $0 \leq N_{re} \leq 3$. The more the retransmission occurs, the lower the throughput will be. Once the retransmission times is larger than three, the data will be discarded and the throughput of TTI will be zero.

4.7 Energy Efficiency

We adopt the bit per Joule as the performance metric which is widely used in the world. Denote T_{total} and P_{total} as the overall system throughput and the total system power consumption, respectively. The energy efficiency metric is defined as:

$$EE(bits/Joule) = \frac{T_{total}(bits/s)}{P_{total}(W)}. \tag{4.30}$$

The EE metric shows us how many bits can be transmitted when one Joule is consumed. Based on (4.30), different systems are able to be evaluated the energy efficiency performance.

CHAPTER 5

Tradeoff Design of Spectral and Energy Efficiency in HetNet Systems

The goal of this chapter is to evaluate the spectral and energy efficiency of hierarchical base station cooperation techniques in HetNet environment and propose a system design methodology for energy-efficient transmission. Because almost 80% of overall system power consumption is attributed to radio access network, we focus on two aspects of BSs, i.e., system architecture and cooperative transmission techniques.

5.1 System Architectures

For system architectures, we consider two factors: RRH deployment and sector antenna architectures. The RRH can provide additional signal power to UEs by cooperating with macro- cell. It plays a vital role in enhancing signal quality. Therefore, we want to investigate the suitable location and the number of RRHs to improve spectral and energy efficiency of the system. If RRHs are placed close to the macro-cell, cell-edge UEs will barely benefit from RRHs due to the long distance. On the contrary, if RRHs are deployed nearly at cell margin, it might cause strong interference to the cell-edge UEs of adjacent cells. In addition, we are interested in the relation of the cooperative RRHs quantity with system performance. Intuitively, increasing RRHs seems to improve signal quality more. However, it also causes more interference to

other cells and consumes power. Hence, finding a moderate numbers of RRHs or even how to decide the serving RRH is important.

Sector antenna architectures have various antenna patterns causing various transmit power distribution, and having different impact on the system performance. We consider the following three types of sector antenna architectures, as shown in Fig. 5.1.

(1) Diamond shape: Each BS is equipped with three 120° directional antennas, and the 3 dB power attenuation angle is set at 70°.

(2) Pentagon shape: Basically, this architecture has the same antenna pattern as diamond shape, but central antenna beams are rotated by a certain angle, which makes a different cell sectorization figure from diamond shape to pentagonal shape.

(3) Narrow beam: Each BS is equipped with three 60° directional antennas, and the 3 dB power attenuation angle is set at 30° [29].

Three adjacent central antenna beams direction of diamond-shape architecture meet at the same point. Thus, cell-edge UEs are easily affected by adjacent cells. However, because the pentagon shape are rotated by a certain angle, it causes fewer interference to other cells. Compared with two other types, the narrow beam can further reduce ICI because the virtual cellular figuration matches realistic cellular figuration better, and thus neighboring sectors cause less interfere to each other.

5.2 CoMP Transmission Techniques

In conventional MIMO systems, cell-edge UEs are more easily interfered by adjacent cells than cell-center UEs. In order to improve signal quality of cell-edge UEs, we deploy small cells within the cell to cooperate with the macro-cell processing signal

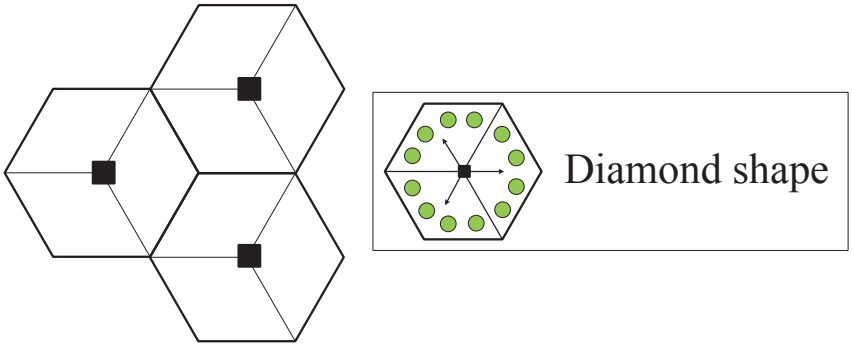

(a) Diamond shape.

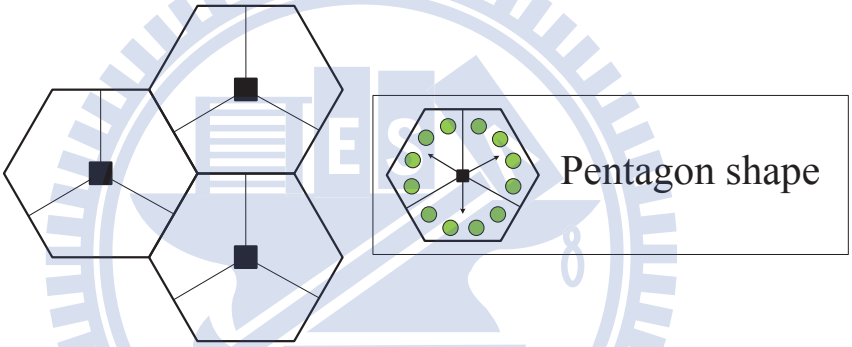

(b) Pentagon shape.

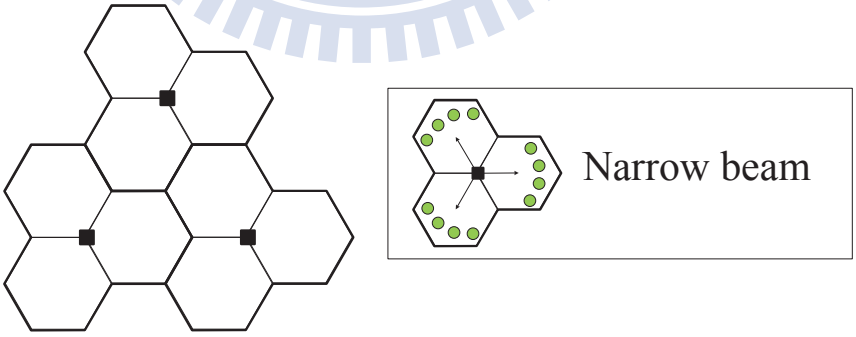

(c) Narrow beam.

Figure 5.1: Sector antenna architectures.

jointly, which is called intra-site CoMP. In this way, the signal strength of cell-edge UE can be enhanced through the additional cooperative signal from small cells. In our work, joint processing (JP) technique is adopted in the intra-site level CoMP transmission. To further mitigate the interference from adjacent cells, we also consider the inter-site cooperation. Therefore, we introduce two other neighboring cells to cooperate with the observing cell. Fig. 5.2 illustrates the two types of coordination schemes mentioned above. For the inter-site level CoMP, we compare inter JP and

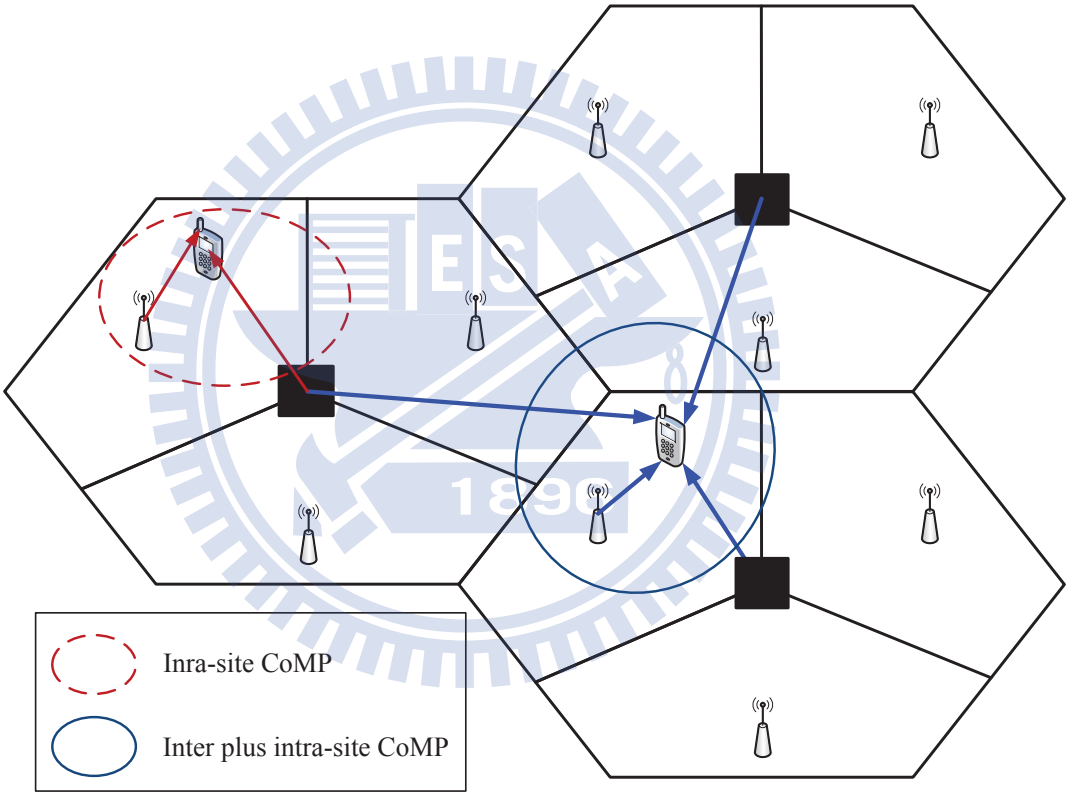

Figure 5.2: Two kinds of CoMP schemes.

inter CS/CB in addition to the intra-site JP. Three cells serve an UE jointly at the same time in JP. For CS/CB, each cell serves a individual UE, but manages to mitigate interference to UEs in other cells. It is not easy to predict which one is

better. Therefore, we compare performances of two schemes by simulation to find the best joint level transmission scheme.

5.3 Design Procedures

Fig. 5.3 shows the following steps to seek the optimal design for energy-efficient transmission in HetNet environment. Firstly, we start from the intra-site transmission level. We evaluate the system performance under different RRH locations and sector antenna architectures to learn the best setting. In these steps, we choose the best one with the highest spectral efficiency. Since power consumption of each setting is the same as others, spectral efficiency and energy efficiency are positively correlated. Followed by the previous settings, both cell throughput and energy efficiency of various number of RRHs are compared and examined to determine the better performance tradeoff. Hence, the number of RRHs to cooperate with the macro-cell can be determined to maximize EE. In this step, we determine the best one by energy efficiency. Spectral efficiency and energy efficiency can be negatively correlated because increasing RRHs consumes more power. After obtaining the best system architecture for the intra-site coordinated transmission, we examine different inter-site and intra-site CoMP transmission schemes to determine the most energy-efficient setting. We also select the scheme with the best capacity in this step. Then, once we know the best combination of intra and inter CoMP schemes, the proposed joint design of system architectures and CoMP transmission schemes for HetNet system is revealed.

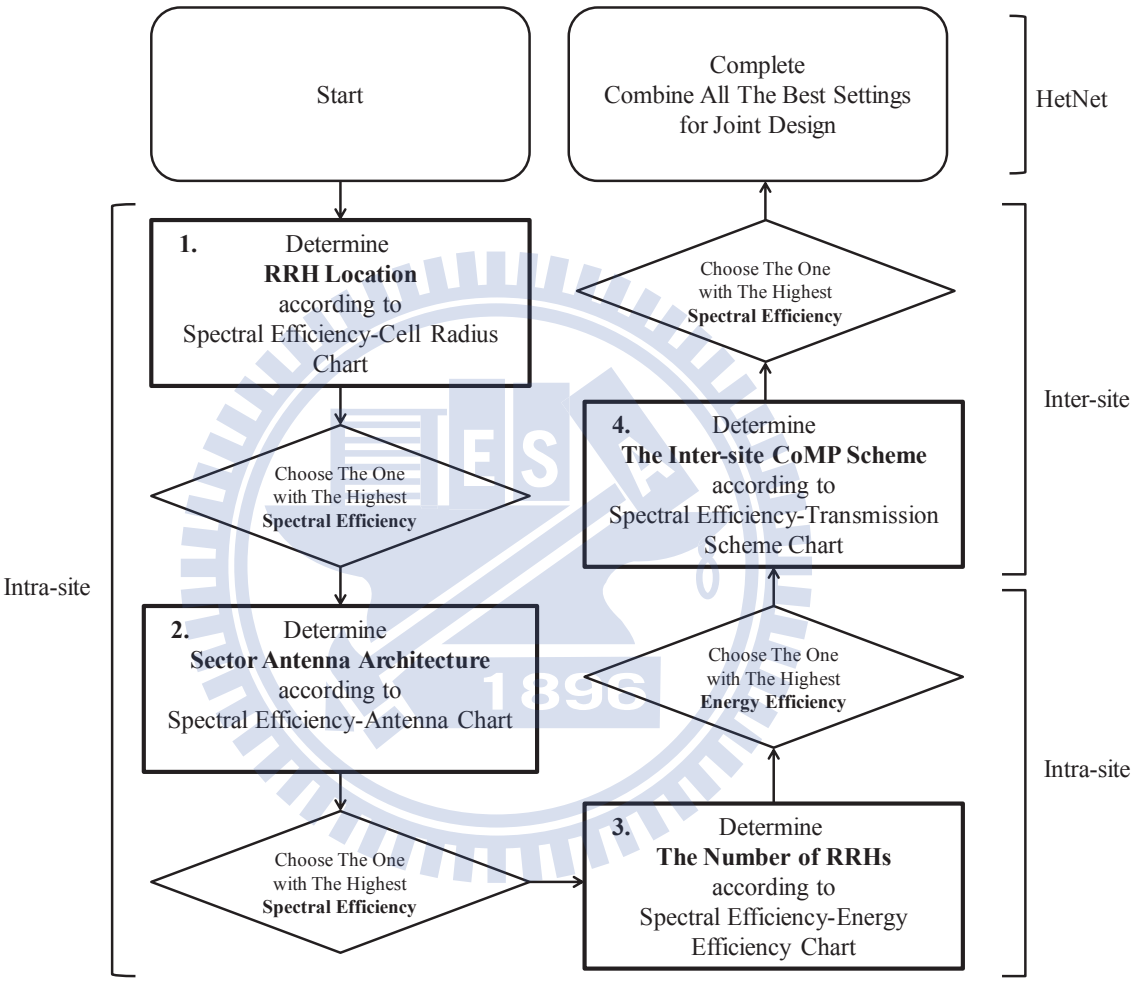

Figure 5.3: Joint design procedure for energy-efficient transmission.

CHAPTER 6

Numerical Results

6.1 Simulation Assumptions

According to [11] and [19], simulation parameter settings are listed in Table 6.1. Our simulation environment is 3GPP case 1, and the frequency division duplex (FDD) transmission mode is adopted. The cellular system consists of nineteen macro-cells with hexagonal grid, and each cell is divided into three sectors. Besides, the inter site distance (ISD) is 500 meters. The center frequency (CF) is 2 GHz, and the whole bandwidth is 10 MHz with 9 MHz available bandwidth. The pathloss and shadowing effect are considered, and the channel model is the SCM urban macro with high spread. The penetration loss is 20 dB. 10 UEs are uniformly distributed in each sector of the central cell, and the speed of UE is 3 km/hr. RRHs are equally spaced in the macro-cell coverage and share the same cell ID with the macro-cell. All 57 sectors are in the same frequency band, and the whole system is synchronized. Full buffer traffic mode is adopted. The maximum retransmission times is three.

6.2 Simulation Baseline

In order to evaluate the performance of heterogeneous CoMP networks, we set the SU-MIMO system as the comparison baseline. We list our simulation results and

Table 6.1: **Simulation Parameters**

Parameter	**Value**
Duplex Method	FDD
DL Transmission Scheme	OFDMA
Number of Available Subcarriers	600
Transmit Antennas	2
Receive Antennas	2
ISD	500 meters
Macro-cell Number	19
UE Distribution	Uniform in all cells
Frequency Reuse	1
Number of UE per Sector	10
UE Speed	3 km/hr
Network Synchronization	Synchronized
Scheduling Method	Proportional fair
HARQ	Max 4 transmissions
Channel Estimation	Ideal
Transmit Power	Macro: 46 dBm RRH: 30 dBm
Noise Power Density	−174 dBm/Hz
Traffic Model	Full buffer
Channel Model	SCM urban macro
Antenna Pattern (Horizontal)	$A_H(\phi) = -\min\left[12\left(\frac{\phi}{\phi_{3dB}}\right), A_m\right]$ $\phi_{3dB} = 70°, A_m = 25$ dBm
Antenna Pattern (Vertical)	$A_V(\theta) = -\min[12(\frac{\theta-\theta_{etilt}}{\theta_{3dB}})^2, SLA_v]$ $\theta_{etilt} = 15°, \theta_{3dB} = 10°, SLA_v = 20$ dBm
Penetration Loss	20 dB
Pathloss Model	Macro: $128.1 + 37.6 \cdot \log_{10}(d)$, d in km RRH: $140.7 + 36.7 \cdot \log_{10}(d)$, d in km
Shadowing Model	Lognormal with zero mean and 8 dB standard deviation

other results of the 3GPP technical report in Table 6.2 [30]. The maximal value of average spectral efficiency in 3GPP specification is 2.47 (bps/Hz/cell), and the minimal value is 2.14 (bps/Hz/cell). As for cell-edge spectral efficiency, the maximal value in 3GPP specification is 0.072 (bps/Hz/cell), and the minimal value is 0.100 (bps/Hz/cell). The average and cell-edge spectral efficiency of our work are 2.41 (bps/Hz/cell) and 0.083 (bps/Hz/cell), respectively. Our simulation results lie within the interval between the maximal and the minimal value in the 3GPP technical report.

Table 6.2: **2x2 SU-MIMO Simulation Results Comparison**

	Min value of 3GPP Spec.	**Our Work**	**Max value of 3GPP Spec.**
Cell Average Spectral Efficiency (bps/Hz/cell)	2.14	2.41	2.47
5% Cell-edge Spectral Efficiency (bps/Hz/UE)	0.072	0.083	0.100

6.3 Intra-site CoMP

6.3.1 Effect of RRH Deployment

We notice that different RRH positions yield various system performances. In this section, we adopt the diamond shape antenna architecture first. As we can see from Fig. 6.1, when RRHs are placed 144.3 meters (0.5R) away from the macro-cell, the SE is higher than any other positions regardless of the number of RRHs. If RRHs are too close to the macro-cell, most UEs are out of RRH coverage. In contrast, if

RRHs are located near by the cell boarder, it will cause interference to cell-edge UEs in other cells. Since the power consumption is fixed despite of different distances between the RRH and macro-cell, EE is also the highest when RRHs are deployed at 0.5R. The similar trend of SE polygonal line can be seen in EE at Fig. 6.2. Thus, RRHs are always deployed 144.3 meters (0.5R) away from the macro-cell in the following simulations so as to achieve better SE and EE. The EE gain of 4 RRHs over SU-MIMO is 12 %, and the SE gain of 4 RRHs is 5.4 %.

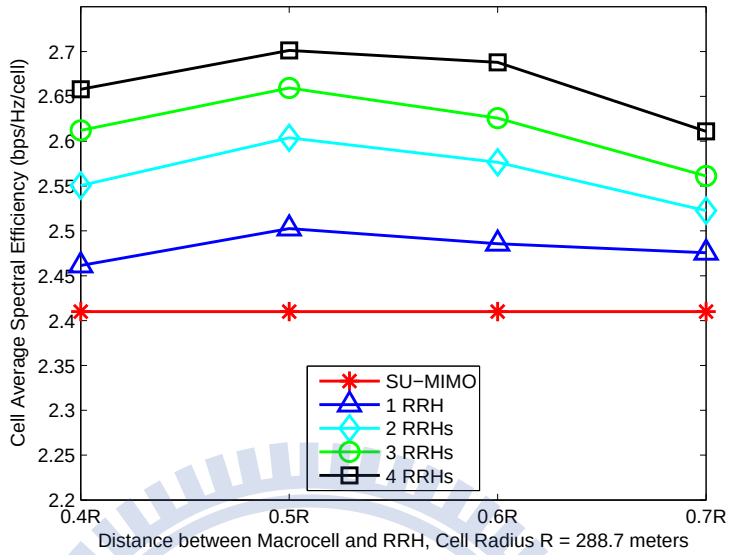

Figure 6.1: Comparison of spectral efficiency for different RRH locations.

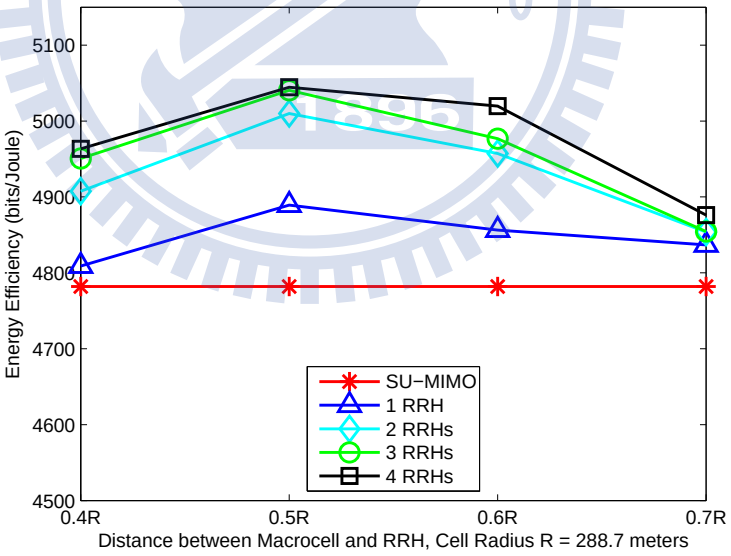

Figure 6.2: Comparison of energy efficiency for different RRH locations.

6.3.2 Effect of Cell Architecture

Different cell structures have various impacts on the system performance. Spectral and energy efficiency comparison of different system architectures are shown in Figs. 6.4 and 6.3. We find that all the cell architectures have the same trend in both SE and EE curve. The best location for RRH to achieve the highest SE and EE is at 0.5-0.6R, where R is the cell radius. Moreover, the performance of narrow beam is the best, and the diamond shape is the worst. Because three adjacent directional antennas are facing toward the same point in diamond shape architecture, it will cause larger interference than the other two kinds of antenna pattern. As for narrow beam, it can avoid causing interference to other cells effectively, and thus it has the best system performance. When RRHs are deployed at 0.5R, both SE and EE are maximum. The spectral efficiency of narrow beam is 2.8660 (bps/Hz/cell), which is the highest. The second one is pentagon shape, which is 2.8363 (bps/Hz/cell). The diamond shape has the lowest energy efficiency, 2.7012 (bps/Hz/cell). The SE gain of the narrow beam over diamond shape is up to 7.9%, and the gain of the pentagon-shape is 5.9%. The energy efficiency of narrow beam is 5352 (bits/Joule), which is also the highest. The second one is pentagon shape, which is 5296 (bits/Joule). The diamond shape has the lowest energy efficiency, 5044 (bits/Joule). The SE gain of narrow beam over the diamond shape is up to 6.1%, and the gain of pentagon shape is 4.9%.

6.3.3 Tradeoff between Spectral and Energy Efficiency

Based on Fig. 6.5, we observe that the system throughput is growing with the number of RRHs. However, EE does not necessarily increase with the amount of RRHs. On the contrary, EE stops increasing when RRHs are up to a certain number. For instance, the system with 8 RRHs has the highest SE, but the EE is just 5279 (bits/Joule), which is lower than the EE of 4 RRHs, e.g., 5357 (bits/Joule). Ac-

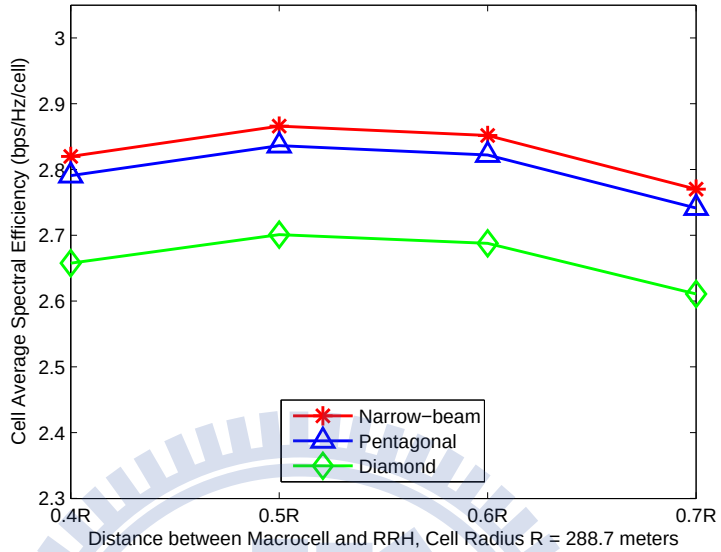

Figure 6.3: Comparison of spectral efficiency for different system architectures.

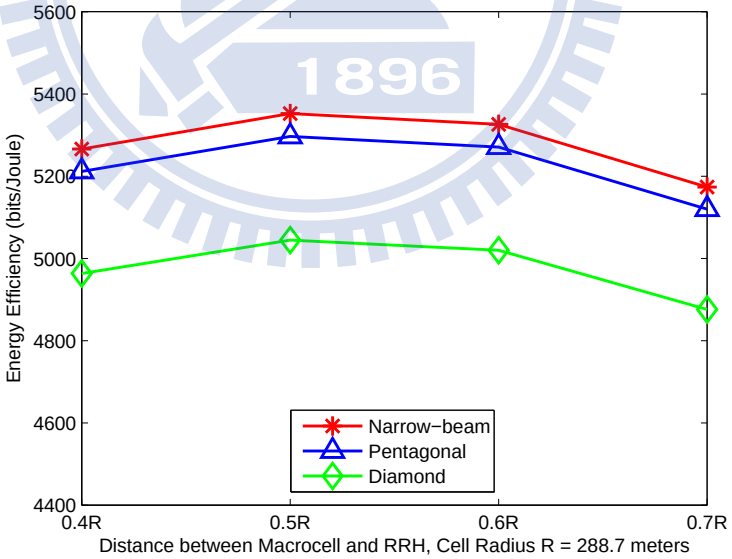

Figure 6.4: Comparison of energy efficiency for different system architectures.

cording to (1.5), when the increased margin of numerator is smaller than that of the denominator, the fraction becomes smaller. That is to say, the gain in throughput is unable to compensate the additional power dissipation, which causes EE degradation. As the number of RRHs exceeds 4, the gained margin gets smaller. It's true that placing more RRHs improves higher spectral efficiency. However, interferences from RRHs also increase, thereby degrading system throughput. Therefore, although the system with 4 RRHs does not have the highest SE, its EE is the best. In fact, no matter how many RRHs are, heterogeneous CoMP systems always outperform the conventional SU-MIMO system in terms of SE and EE. Namely, although additional power is needed for the intra-site CoMP scheme, energy can be utilized more efficiently by the intra-site CoMP scheme. We list gains in spectral efficiency and accordingly induced energy efficiency variation at Table 6.3.

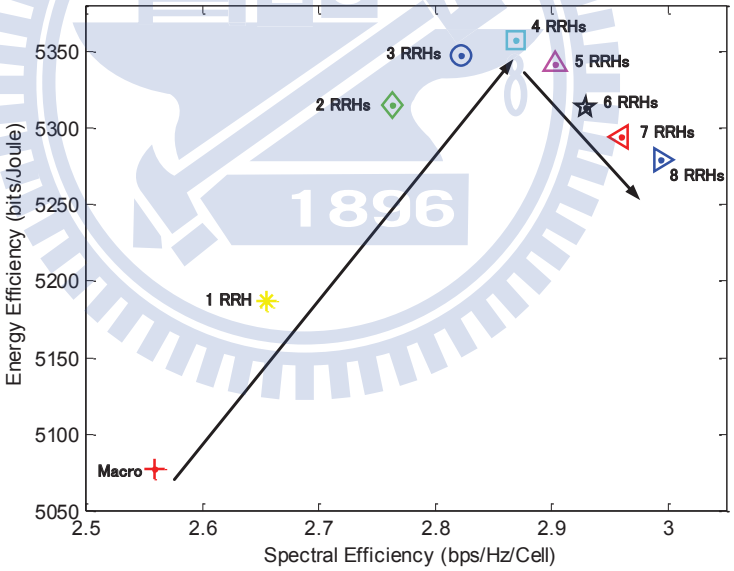

Figure 6.5: Tradeoff between spectral efficiency and energy efficiency of the intra-site CoMP scheme.

Table 6.3: **Relative gains of intra-site CoMP schemes**

Scheme	**SE gain** (%)	**EE gain** (%)	**Consumed Power** (W)
SU-MIMO	0	0	4535
Intra 1RRH	3.92	2.17	4606
Intra 2RRHs	8.24	4.69	4677
Intra 3RRHs	10.59	5.34	4748
Intra 4RRHs	12.16	5.55	4819
Intra 5RRHs	13.37	5.22	4890
Intra 6RRHs	14.51	4.65	4961
Intra 7RRHs	16.08	4.27	5032
Intra 8RRHs	17.25	3.98	5102

6.4 Inter plus Intra-site CoMP

In the previous section, we demonstrate the overall system throughput and energy efficiency in intra-site CoMP scenario where neighboring cells still cause great interference. In order to further reduce the interference, we introduce neighboring sectors to perform joint transmission or coordinated scheduling/beamforming with the original base site. The cooperation of intra-site CoMP scheme is limited only in one sector, while the cooperation of inter-site CoMP scheme can be across sectors. At the beginning, we evaluate system performances of inter-site CoMP schemes without the intra-site coordination and compare that with the conventional SU-MIMO system, as shown in Fig. 6.6. Despite of additional power for cooperation, the large gain in spectral efficiency can improve energy efficiency enormously. For the inter-site CS/CB CoMP, the energy efficiency is up to 5759 (bits/Joule), and it achieves 16.3% gain over the SU-MIMO system. In addition, the inter-site JP CoMP can also achieve about 13.5% over the conventional system.

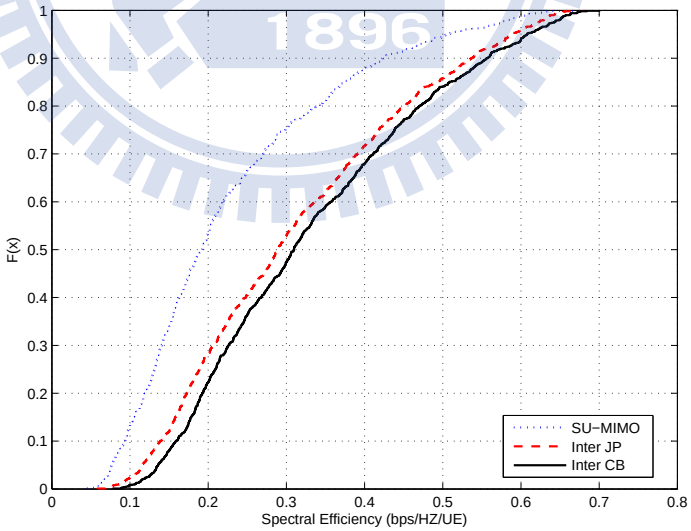

Figure 6.6: Spectral efficiency comparison of different transmission schemes.

Next we combine inter and intra-site CoMP techniques to improve signal quality of cell-edge UEs and further mitigate interferences from adjacent cells. In the single UE case, the inter plus intra-site CoMP scheme outperforms the SU-MIMO transmission scheme and the intra-site CoMP scheme in terms of both SE and EE, as shown in Fig. 6.7 and Fig. 6.8. The SE of SU-MIMO, intra-site JP, inter JP plus intra-site JP, and inter CS/CB plus intra-site JP are 2.41 (bps/Hz), 2.86 (bps/Hz), 3.12 (bps/Hz), 3.19 (bps/Hz), respectively. The EE of SU-MIMO, intra-site JP, inter JP plus intra-site JP, and inter CS/CB plus intra-site JP, are 5077 (bits/Joule), 5352 (bits/Joule), 5775 (bits/Joule), 5915 (bits/Joule), respectively. We set the SU-MIMO system as comparison baseline. The SE gain of intra-site JP, inter JP plus intra-site JP, and inter CS/CB plus intra-site JP, are 12%, 25.8%, and 28.7%, respectively. On the other hand, intra-site JP, inter JP plus intra-site JP, and inter CS/CB plus intra-site JP can achieve 5.4%, 17.4%, 20.1% EE gain, respectively. For the multiple UE case, we set the MU-MIMO as comparison baseline. Fig. 6.9 shows that SE gain of intra-site JP, inter JP plus intra-site JP, and inter CS/CB plus intra-site JP, are 29.7%, 39.1%, and 47%, respectively. On the other hand, Fig. 6.10 shows that intra-site JP, inter JP plus intra-site JP, and inter CS/CB plus intra-site JP can achieve 23.2%, 29.8%, 37.2% EE gain, respectively.

Because the intra-site CoMP can only enhance the signal by deploying cooperative small cells, the inter-cell interference which put great impacts on cell-edge UEs still exists. Nevertheless, because the inter-site CoMP can reduce interferences from nearby macro-cells, the signal quality will be improved significantly. In summary, the inter-site CS/CB plus intra-site JP with 4 RRHs is the most efficient CoMP scheme.

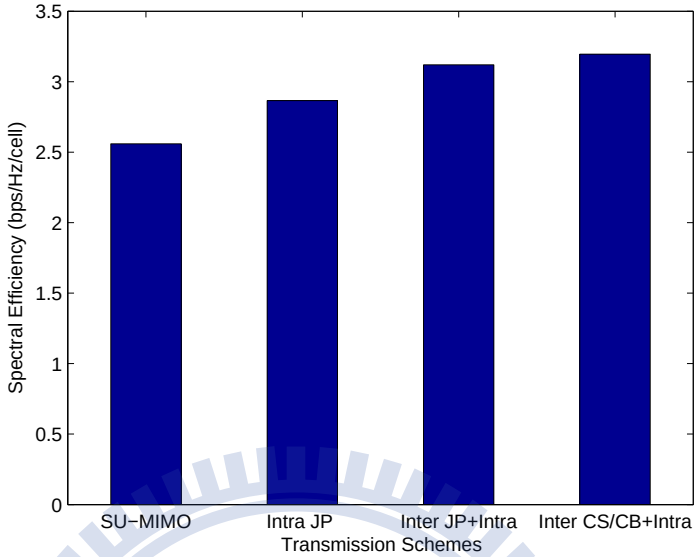

Figure 6.7: Comparison of spectral efficiency for different transmission schemes in the single UE case.

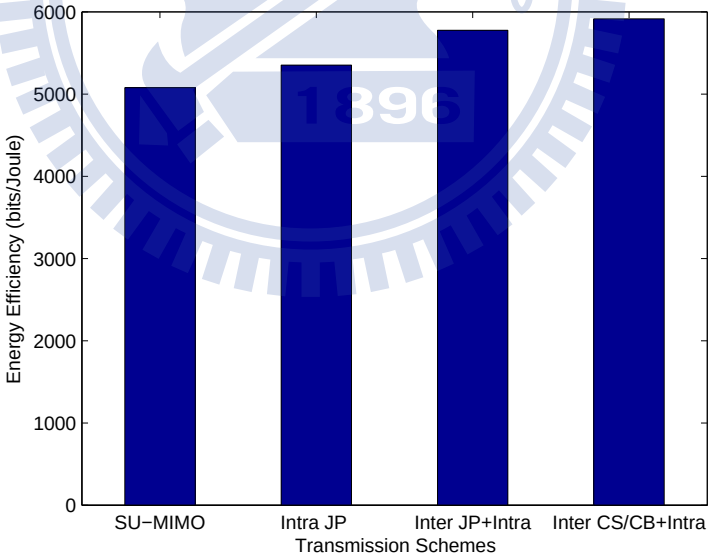

Figure 6.8: Comparison of energy efficiency for different transmission schemes in the single UE case.

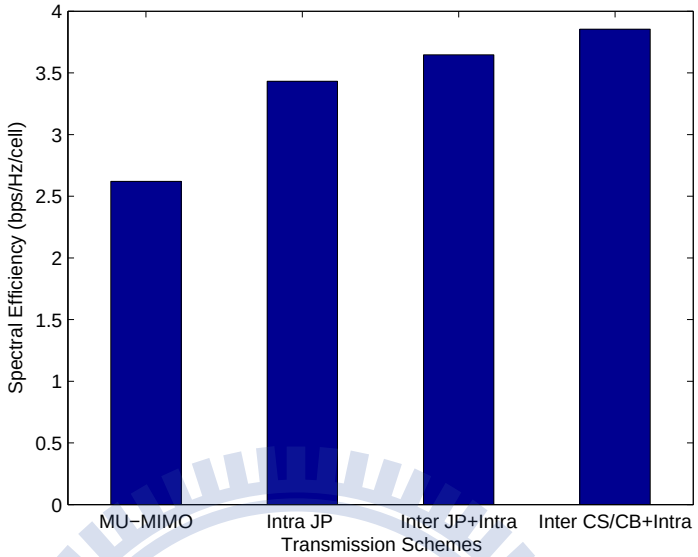

Figure 6.9: Comparison of spectral efficiency for different transmission schemes in the multiple UE case.

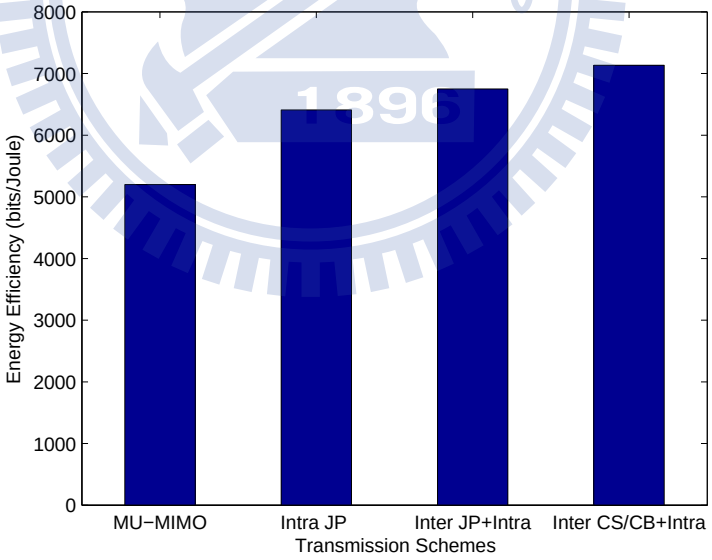

Figure 6.10: Comparison of energy efficiency for different transmission schemes in the multiple UE case.

6.5 Reference Signal Received Power-Based RRH Selection

According to the previous section, 4 cooperative RRHs yield the highest energy efficiency. However, not every RRH can bring obvious merit to the UE. If a RRH is far away from the served UE, the received signal quality will be very poor. Hence, the SE improvement offered by RRHs is little. Moreover, increasing the number of RRH causes more interferences to UEs in other cells. If we select a RRH which transmits the largest reference signal received power (RSRP) to the UE, and switch off the other RRHs in the same sector, both SE and EE will be further improved due to less interferences and operation power consumption for RRHs. Figs. 6.11 and 6.12 compare various CoMP schemes with different density of RRH for selection. Besides, we only choose the RRH with the best signal quality to serve UEs jointly with the macro-cell. We find that both metrics increase with the density of RRH because UEs are more likely to be served by a better RRH with the increasing RRH density. However, the margin of performance gain of deploying 4 RRHs is the highest. When the number of RRH for selection exceeds 4, the margin of performance gain becomes smaller. Take the EE margin from 3 to 4 RRHs and the EE margin from 6 to 7 RRHs in intra-site CoMP case as an example. The differences are 176 (bits/Joule) and 11 (bits/Joule), respectively. The same phenomenon can be also observed in the intra JP plus inter JP and the intra JP plus inter CS/CB scheme. Therefore, selecting a serving RRH from 4 RRHs is the best way to make better energy utilization.

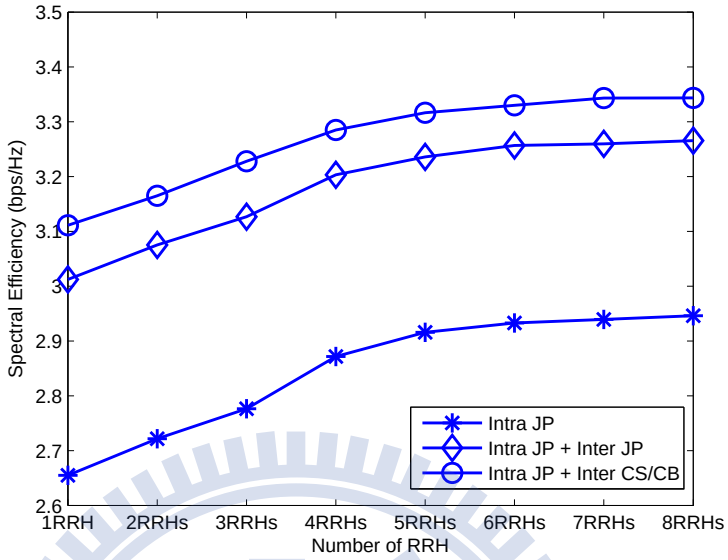

Figure 6.11: Comparison of spectral efficiency for different RRH density with selection.

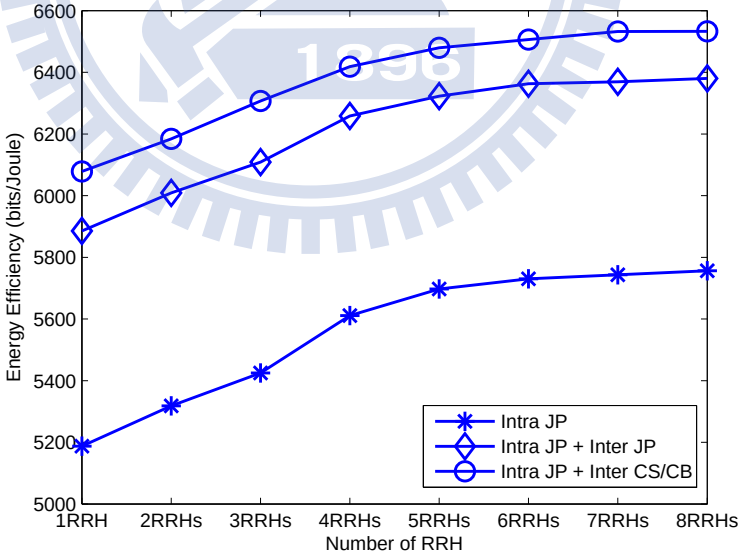

Figure 6.12: Comparison of energy efficiency for different RRH density with selection.

CHAPTER 7

Conclusions

7.1 Thesis Summary

In this thesis, we have evaluated the spectral efficiency and energy efficiency of hierarchical base station cooperation techniques in heterogeneous networks of the 3GPP LTE-A system. We proposed a joint system design methodology of system architectures and cooperation schemes for energy-efficient transmission. We focused on two aspects of BSs, including system architectures and CoMP transmission techniques. In terms of system architectures, we suggested that RRHs should be deployed at the distance of 0.5-0.6R (R is the macro cell radius) from the macro cell and adopting narrow beam antenna architecture to achieve both the highest spectral and energy efficiency. We also discovered that there exists spectral-energy efficiency tradeoff for small cell density. It is true that increasing cooperative RRHs yields higher capacity. However, energy efficiency start declining when the number of RRHs is larger than four. The reason is that the gain in system throughput cannot compensate the additional power consumption induced by the increased small cells. Moreover, we can exploit energy more efficiently by applying the reference signal received power-based RRH selection method. As for CoMP transmission schemes, the cooperation among BSs not only enhances the overall throughput, but also improves the energy efficiency compared to conventional SU-MIMO systems. We considered different levels of CoMP schemes

jointly to obtain an optimal combination. In our cases, the best coordination scheme is the inter CS/CB plus intra-site JP CoMP scheme. The proposed joint design for HetNet systems has been revealed by combining the best settings of all aspects. In summary, we offered the knowledge of how to deploy an energy-efficient system.

7.2 Suggestions for Future Research

For the future research of the thesis, we provide the following suggestions to extend our work. More precise power consumption models should be taken into consideration to match realistic situations. For instance, we only consider the number of cooperation BSs in the signal processing power consumption model for inter-site CoMP. However, inter-site CoMP techniques include JP and CS/CB, and the corresponding feedback overhead information as well as the computational complexity will not be the same. Therefore, different schemes may induce various power consumption, and thus it is worthy of making a further discussion.

Bibliography

[1] E. Oh, B. Krishnamachari, X. Liu, and Z. Niu, "Toward dynamic energy-efficient operation of cellular network infrastructure," *IEEE Commun. Magazine*, vol. 49, no. 6, pp. 56–61, Jun. 2011.

[2] W. Vereecken, W. Van Heddeghem, M. Deruyck, B. Puype, B. Lannoo, W. Joseph, D. Colle, L. Martens, and P. Demeester, "Power consumption in telecommunication networks: overview and reduction strategies," *IEEE Commun. Magazine*, vol. 49, no. 6, pp. 62–69, Jun. 2011.

[3] Z. Hasan, H. Boostanimehr, and V. K. Bhargava, "Green cellular networks: a survey, some research issues and challenges," *IEEE Communications Surveys Tutorials*, vol. 13, no. 4, pp. 524–540, 2011.

[4] H. Bogucka and A. Conti, "Degrees of freedom for energy savings in practical adaptive wireless systems," *IEEE Commun. Magazine*, vol. 49, no. 6, pp. 38–45, Jun. 2011.

[5] Q. Wang, D. Jiang, G. Liu, and Z. Yan, "Coordinated multiple points transmission for LTE-Advanced systems," in *Proc. International Conference on Wireless Communications, Networking and Mobile Computing*, pp. 1–4, Sep. 2009.

[6] L. C. Wang and C. J. Yeh, "A three-cell coordinated network MIMO with fractional frequency reuse and directional antennas," in *Proc. IEEE International Conference on Communications*, pp. 1–5, May 2010.

[7] A. Barbieri, P. Gaal, S. Geirhofer, T. Ji, D. Malladi, Y. Wei, and F. Xue, "Coordinated downlink multi-point communications in heterogeneous cellular networks," in *Proc. Information Theory and Applications Workshop*, pp. 7–16, Feb. 2012.

[8] Y. Chen, S. Zhang, S. Xu, and G. Y. Li, "Fundamental trade-offs on green wireless networks," *IEEE Commun. Magazine*, vol. 49, no. 6, pp. 30–37, Jun. 2011.

[9] G. Miao, N. Himayat, Y. Li, and A. Swami, "Cross-layer optimization for energy-efficient wireless communications: a survey," *Wiley Journal Wireless Communications and Mobile Computing*, vol. 9, no. 4, pp. 529–542, Apr. 2009.

[10] C. Han, T. Harrold, S. Armour, I. Krikidis, S. Videv, P. M. Grant, H. Haas ,J. S. Thompson, I. Ku, C. Wang, T. A. Le, M. R. Nakhai, J. Zhang, and L. Hanzo, "Green radio: radio techniques to enable energy-efficient wireless networks," *IEEE Commun. Magazine*, vol. 49, no. 6, pp. 46–54, Jun. 2011.

[11] 3GPP, "Technical specification group radio access network; coordinated multi-point operation for LTE physical layer aspects," 3GPP, Tech. Rep. TR 36.819 V11.0.0, Dec. 2011.

[12] C. Khirallah, J. S. Thompson, and D. Vukobratovic, "Energy efficiency of heterogeneous networks in LTE-Advanced," in *Proc. IEEE Wireless Communications and Networking Conference Workshops*, pp. 53–58, Apr. 2012.

[13] L. Saker, S. E. Elayoubi, L. Rong, and T. Chahed, "Capacity and energy efficiency of picocell deployment in LTE-A networks," in *Proc. IEEE Vehicular Technology Conference*, pp. 1–5, May 2011.

[14] T. Q. S. Quek, W. C. Cheung, and M. Kountouris, "Energy efficiency analysis of two-tier heterogeneous networks," in *Proc. European Wireless Conference*, pp. 1–5, Apr. 2011.

[15] F. Cao and Z. Fan, "The tradeoff between energy efficiency and system performance of femtocell deployment," in *Proc. International Symposium on Wireless Communication Systems*, pp. 315–319, Sep. 2010.

[16] Y. Liang, A. Goldsmith, G. Foschini, R. Valenzuela, and D. Chizhik, "Evolution of base stations in cellular networks: denser deployment versus coordination," in *Proc. IEEE International Conference on Communications*, pp. 4128–4132, May 2008.

[17] A. J. Fehske, P. Marsch, and G. P. Fettweis, "Bit per joule efficiency of cooperating base stations in cellular networks," in *Proc. IEEE GLOBECOM Workshops*, pp. 1406–1411, Dec. 2010.

[18] C. Khirallah, D. Vukobratovic, and J. Thompson, "On energy efficiency of joint transmission coordinated multi-point in LTE-Advanced," in *Proc. International ITG Workshop on Smart Antennas*, pp. 54–61, Mar. 2012.

[19] 3GPP, "Evolved universal terrestrial radio access (E-UTRA); further advancements for E-UTRA physical layer aspects," 3GPP, Tech. Rep. TR 36.814 V9.0.0, Mar. 2010.

[20] F. Khan, *LTE for 4G Mobile Broadband: Air Interface Technologies and Performance*. Cambridge University Press, 2009.

[21] Documents provided by Chunghwa telecom laboratories.

[22] Q. Wang, D. Jiang, J. Jin, G. Liu, Z. Yan, and D. Yang, "Application of BBU+RRU based CoMP system to LTE-Advanced," in *Proc. IEEE International Conference on Communications Workshops*, pp. 1–5, Jun. 2009.

[23] NTT DOCOMO, Alcatel-Lucent, Alcatel-Lucent Shanghai Bell, Ericsson, and Telecom Italia, "Base station power model," 3GPP, Tech. Rep. R1-113495, Oct. 2011.

[24] G. Auer, V. Giannini, C. Desset, I. Godor, P. Skillermark, M. O. M. A. Imran, D. Sabella, M. J. Gonzalez, O. Blume, and A. Fehske, "How much energy is needed to run a wireless network?" *IEEE Wireless Communications Magzine*, vol. 18, no. 5, pp. 40–49, Oct. 2011.

[25] 3GPP, "Physical layer aspects for evolved universal terrestrial radio access (E-UTRA)," 3GPP, Tech. Rep. TR 25.814 V7.1.0, Sep. 2006.

[26] 3GPP, "Evolved universal terrestrial radio access (E-UTRA) physical layer procedures," 3GPP, Tech. Rep. TS 36.213 V9.3.0, Sep. 2010.

[27] J. C. Ikuno, M. Wrulich, and M. Rupp, "System level simulation of LTE networks," in *Proc. IEEE Vehicular Technology Conference*, pp. 1–5, May 2010.

[28] Y. J. Liu, T. T. Chiang, and L. C. Wang, "Physical layer performance calibration for 3GPP LTE-A systems," in *Proc. IEEE Asia Pacific Wireless Communication Symposium*, Aug. 2011.

[29] L. C. Wang, "A new cellular architecture based on an interleaved cluster concept," *IEEE Transactions on Vehicular Technology*, vol. 48, no. 6, pp. 1809–1818, Nov. 1999.

[30] NTT DOCOMO, "Summary of evaluation results for 3GPP requirements," 3GPP, Tech. Rep. R1-100823, Jan. 2010.

Vita

Tsung-Chan Hsieh received his B.S. degree from the Department of Communication Engineering, National Chiao-Tung University, Taiwan, R.O.C., in 2010. From July 2010 to August 2012, he worked his Master degree in the Mobile Communications and Cloud Computing Lab at the Institute of Communications Engineering at National Chiao-Tung University. His research interests are in the field of wireless communications.